











## The Sun’s Alfvén Surface: Recent Insights and Prospects for the *Polarimeter to Unify the Corona and Heliosphere* (PUNCH)

Steven R. Cranmer<sup>1</sup>  · Rohit Chhiber<sup>2,3</sup>  ·  
Chris R. Gilly<sup>4,1</sup>  · Iver H. Cairns<sup>5</sup>  ·  
Robin C. Colaninno<sup>6</sup>  ·  
David J. McComas<sup>7</sup>  · Nour E. Raouafi<sup>8</sup>  ·  
Arcadi V. Usmanov<sup>2,3</sup>  ·  
Sarah E. Gibson<sup>9</sup>  · Craig E. DeForest<sup>4</sup> 

© The author(s) ●●●●

**Abstract** The solar wind is the extension of the Sun’s hot and ionized corona, and it exists in a state of continuous expansion into interplanetary space. The radial distance at which the wind’s outflow speed exceeds the phase speed of Alfvénic and fast-mode magnetohydrodynamic (MHD) waves is called the Alfvén radius. In one-dimensional models, this is a singular point beyond which most fluctuations in the plasma and magnetic field cannot propagate back down to the Sun. In the multi-dimensional solar wind, this point can occur at different distances along an irregularly shaped “Alfvén surface.” In this article, we review the properties of this surface and discuss its importance in models of solar-wind acceleration, angular-momentum transport, MHD waves and turbulence, and

---

✉ S.R. Cranmer  
[steven.cranmer@colorado.edu](mailto:steven.cranmer@colorado.edu)

- <sup>1</sup> Department of Astrophysical and Planetary Sciences, Laboratory for Atmospheric and Space Physics, University of Colorado, Boulder, CO, USA
- <sup>2</sup> Department of Physics and Astronomy, University of Delaware, Newark, DE, USA
- <sup>3</sup> Heliophysics Science Division, NASA Goddard Space Flight Center, Greenbelt, MD, USA
- <sup>4</sup> Southwest Research Institute, 1050 Walnut Street, Suite 300, Boulder, CO, USA
- <sup>5</sup> School of Physics, University of Sydney, Sydney, NSW 2006, Australia
- <sup>6</sup> Space Science Division, Naval Research Laboratory, Washington, DC 20375, USA
- <sup>7</sup> Department of Astrophysical Sciences, Princeton University, Princeton, NJ 08544, USA
- <sup>8</sup> Johns Hopkins University Applied Physics Laboratory, Laurel, MD, USA
- <sup>9</sup> National Center for Atmospheric Research, 3080 Center Green Drive, Boulder, CO, USA

the geometry of magnetically closed coronal loops. We also review the results of simulations and data analysis techniques that aim to determine the location of the Alfvén surface. Combined with recent perihelia of *Parker Solar Probe*, these studies seem to indicate that the Alfvén surface spends most of its time at heliocentric distances between about 10 and 20 solar radii. It is becoming apparent that this region of the heliosphere is sufficiently turbulent that there often exist multiple (stochastic and time-dependent) crossings of the Alfvén surface along any radial ray. Thus, in many contexts, it is more useful to make use of the concept of a topologically complex “Alfvén zone” rather than one closed surface. This article also reviews how the *Polarimeter to Unify the Corona and Heliosphere* (PUNCH) mission will measure the properties of the Alfvén surface and provide key constraints on theories of solar-wind acceleration.

**Keywords:** Heliospheric base; Sun: corona; Sun: magnetic field

## 1. Introduction

The solar corona is a region of the Sun’s atmosphere defined by its high temperature ( $T > 10^6$  K), and the solar wind is defined mainly by the presence of radially accelerating plasma that reaches supersonic speeds within a few solar radii [ $R_\odot$ ] of the solar surface. The corona is typically observed near the Sun with telescopes, and the solar wind is typically probed further out with in-situ particle and field detectors. Despite these historical differences, these two regions overlap to such an extent that it often makes no sense to specify a dividing line between them. Still, it is known that the strongest forces acting on the plasma undergo a transition from being mostly magnetic, near the Sun, to mostly hydrodynamic – i.e. depending on gas-pressure gradients and nonlinear inertial gas flow terms – far from the Sun. A common way to quantify this transition is to locate the *Alfvén surface*, the place where the radially increasing solar-wind speed [ $u$ ] exceeds the radially decreasing Alfvén speed [ $V_A$ ]. This article provides an overview of the various ways that the Alfvén surface is significant to our understanding of the physics of the heliosphere, and it also discusses past, present, and future attempts to measure its detailed properties.

The topic of this article has been called by a number of different names. One-dimensional and time-steady models talk about an Alfvén radius, an Alfvén point, or an Alfvénic critical point. With multi-dimensional models came the realization that there is no single radial distance that has this property, so the community began discussing the Alfvén surface, or Alfvénic critical boundary, as a closed but nonspherical “bubble.” The synonymous term *heliobase* was also coined as a way to discuss the Alfvén surface’s role as an inner boundary condition for the larger heliosphere (Zhao and Hoeksema, 2010). We will tend to use the symbol  $r_A$  to refer to its heliocentric radial distance, and the regions of the heliosphere with  $r < r_A$  and  $r > r_A$  are called sub-Alfvénic and super-Alfvénic, respectively. The vicinity of  $r \approx r_A$ , which may contain multiple crossings of the point at which  $u = V_A$ , is called the trans-Alfvénic region or Alfvén zone.

The present decade is an exciting time for studies of the Sun’s Alfvén surface. Most notably, *Parker Solar Probe* (PSP: Fox et al., 2016; Raouafi et al., 2023)

has been the first spacecraft to cross it and measure the properties of particles and fields in the sub-Alfvénic region (Kasper et al., 2021). However, an in-situ probe will never be able to measure the global three-dimensional (3D) shape of the Alfvén surface. We anticipate the launch of the *Polarimeter to Unify the Corona and Heliosphere* (PUNCH), a NASA Small Explorer mission that will perform regular, global, deep-field imaging of the accelerating solar wind (DeForest et al., 2022). One of the six main scientific questions to be addressed by the PUNCH mission is: What are the evolving physical properties of the Alfvén surface? PUNCH will produce the first global maps of the time-variable shape of this key boundary region in the heliosphere, and Working Group 1C of the PUNCH Science Team is in the process of preparing to make the most of these measurements. This article provides a snapshot of the current state of the science and a summary of plans for this objective moving forward.

Section 2 of this article discusses several different physical contexts in which the Alfvén surface plays an important role. Section 3 reviews theoretical and observational attempts to measure  $r_A$  itself, and Section 4 speculates about how the PUNCH mission will improve on the existing measurements. Lastly, Section 5 concludes by discussing broader implications for other open questions in heliophysics and astrophysics.

## 2. Definitions and Physical Processes

In Section 2.1, we define the various critical points found in solar wind models, including the Alfvén radius. Then we discuss the importance of the Alfvén radius to some key phenomena in the corona and solar wind, such as angular momentum transport (Section 2.2), the evolution of waves and turbulence (Section 2.3), and the Sun’s open/closed magnetic topology (Section 2.4).

### 2.1. Critical Points in a Time-Steady Wind

Here, we summarize the basics of how the solar wind is understood to accelerate through several critical or singular points of the magnetohydrodynamic (MHD) conservation equations. These points are related to the linear propagation of information through the system; i.e. they describe characteristics of the underlying differential equations that govern the flow. For other insightful reviews of these processes, see, for example, Hundhausen (1972), Sakurai (1990), Lifschitz and Goedbloed (1997), and Owocki (2009).

Parker (1958) solved the time-steady system described by the spherically symmetric hydrodynamic outflow of an isothermal gas, with an equation of motion given by

$$\left[ u - \frac{c_i^2}{u} \right] \frac{du}{dr} = \left[ \frac{2c_i^2}{r} - \frac{GM_\odot}{r^2} \right]. \quad (1)$$

This equation shows how the radial outflow speed  $u(r)$  behaves as a result of both gravity (with gravitational constant  $G$  and solar mass  $M_\odot$ ) and the gas-pressure gradient force (here parameterized by a constant sound speed  $c_i$ ). In

this case, the flow is purely hydrodynamic (no magnetic forces), and the radial acceleration  $du/dr$  remains finite when both terms in square brackets are zero:

$$u_{\text{crit}} = c_i \quad \text{and} \quad r_{\text{crit}} = \frac{GM_{\odot}}{2c_i^2} . \quad (2)$$

This occurs at a “critical radius” that is equivalent to the point where the flow transitions from subsonic ( $u < c_i$ ) to supersonic ( $u > c_i$ ). Note that a hotter corona exhibits a larger value of  $c_i$  and a smaller critical radius. In that case, the outward gas-pressure gradient force exceeds the inward force of gravity sooner. MHD effects play no role in the time-steady momentum equation if the magnetic field vector is oriented parallel to the flow-speed vector. In the Parker (1958) model, this situation would imply a radially oriented field.

Initially, Parker was criticized because the transonic critical-point solution seemed unnaturally “fine-tuned.” Why should the Sun choose the one specific acceleration trajectory that passes through both  $r_{\text{crit}}$  and  $u_{\text{crit}}$ , rather than one of the seemingly infinite other slower wind or “breeze” solutions where, say,  $u < c_i$  everywhere? However, when the actual inner and outer boundary conditions are considered, Parker’s transonic solution turns out to be something akin to a stable attractor – i.e. a solution toward which nonsteady solutions tend to converge – whereas the other solutions exhibit instabilities (see, e.g. Velli, 1994, 2001; Keto, 2020). In addition, the critical point loses some of its importance when including *time-dependent* terms back into the momentum conservation equation (see, e.g. Suess, 1982; Holzer and Leer, 1997). In that case, the system tends to relax to stable transonic acceleration without any regard for the supposed delicateness of the critical solution.

The observational discovery of the supersonic solar wind (Neugebauer and Snyder, 1962) supported Parker’s basic hydrodynamic approach. In the decade that followed, the isothermal model was generalized to allow for radial variations in temperature (Parker, 1964), as well as different temperatures for the ions and electrons (Sturrock and Hartle, 1966) and directionally anisotropic pressure tensors (Hollweg, 1970). Weber and Davis (1967) extended this kind of model to two spatial dimensions; i.e. the equatorial plane defined by the Sun’s rotation axis (see also Belcher and MacGregor, 1976; Sakurai, 1985; Tasnim and Cairns, 2016). Since this scenario allows for the vector magnetic field  $\mathbf{B}$  and flow velocity  $\mathbf{u}$  to no longer be aligned, it can account for the coexistence of forces from both gas-pressure gradients and the magnetic field (i.e.  $\mathbf{J} \times \mathbf{B}$ ). Thus, a generally accelerating outflow may pass through up to *three* distinct critical points corresponding to the phase speeds of obliquely propagating Alfvén waves and fast/slow magnetosonic waves.

Figure 1a shows an example solar-wind model with its three MHD critical points. The radial acceleration is described by the polar coronal-hole model of Cranmer et al. (2007), in which the corona is heated by turbulent dissipation and the wind is also driven by ponderomotive wave-pressure effects. This model has a super-radially expanding magnetic field that is similar to that found in other low-latitude parts of the corona; e.g. equatorial coronal holes and quiet-Sun regions. The one-fluid temperature (i.e. the average of the proton and electron temperatures) is given by an observationally constrained set of curves from multiple

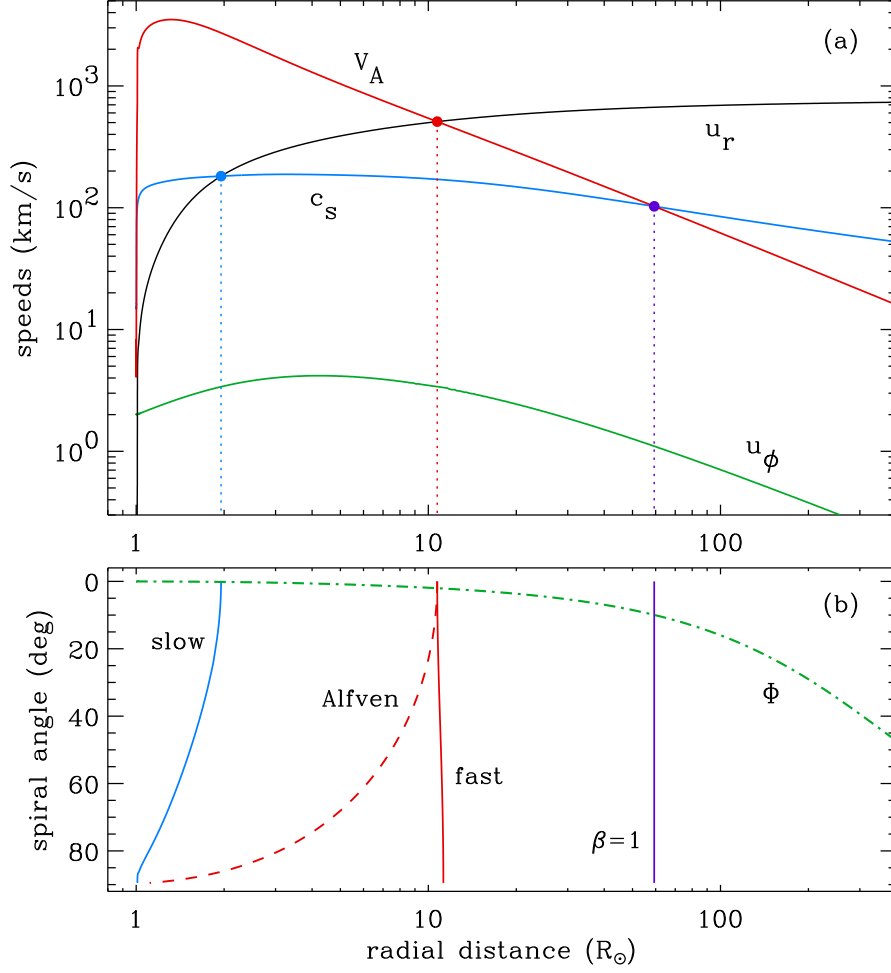


**Figure 1.** Example one-dimensional solar-wind model, with quantities plotted vs. heliocentric radial distance  $r$ , in units of solar radii  $R_\odot$ : (a) radial outflow speed (*black*), sound speed (*blue*), Alfvén speed  $V_{A,r} = B_r/(4\pi\rho)^{1/2}$  (*red*), and azimuthal flow speed (*green*); (b) locations of MHD critical points shown with respect to both  $r$  and the Parker spiral angle  $\Phi$  (*red and blue curves*), plotted alongside the self-consistent  $\Phi(r)$  for the Weber and Davis (1967) model (*green dot-dashed curve*). In both panels, *purple* denotes the  $\beta = 1$  surface (see text).

remote and in-situ measurements in the high-speed solar wind (Cranmer, 2020). Figure 1a also shows the Weber and Davis (1967) solution for the azimuthal velocity in the ecliptic plane,

$$u_\phi(r) = \Omega r \left[ \frac{(M_A r_A / r)^2 - 1}{M_A^2 - 1} \right], \quad (3)$$

where the Alfvénic Mach number  $M_A = u_r/V_{A,r}$  and the angular rotation rate at the Sun’s surface is  $\Omega = 2.9 \times 10^{-6}$  rad s $^{-1}$ . At low heights in the magnetically dominated corona, the rotation is nearly rigid [ $u_\phi \approx \Omega r$ ], which is

related to Ferraro’s (1937) law of iso-rotation. At very large heights, ballistically flowing parcels of solar wind approach a state of angular-momentum conservation [ $u_\phi \propto 1/r$ ]. At intermediate heights, there must be a transition between these two disparate states. Specifically,  $M_A = 1$  at the Alfvén radius, so evaluating  $u_\phi$  requires L’Hôpital’s rule. Making use of the fact that  $\rho M_A^2$  should remain constant along a magnetic flux tube, and approximating the radial dependence of the density as  $\rho \propto r^{-n}$ , one finds that

$$u_\phi(r_A) \approx \Omega r_A \left( \frac{n-2}{n} \right). \quad (4)$$

For the model shown,  $r_A = 10.7 R_\odot$ ,  $n \approx 2.37$ , and Equation 4 correctly gives  $u_\phi \approx 3.3 \text{ km s}^{-1}$ . This is about an order of magnitude smaller than what it would have been if the corona continued to rotate rigidly up to the Alfvén radius.

It should be noted that different studies have used slightly different definitions when determining the locations where  $M_A = 1$ . Weber and Davis (1967) specifically used the ratio of the radial components  $u_r$  and  $V_{A,r}$ , with the latter computed from the radial component of the magnetic field  $B_r$ . Bandyopadhyay et al. (2022) used  $u_r$  and the magnitude of  $B$ , Cohen (2015) and Chhiber et al. (2022) used the magnitudes  $u$  and  $B$ , and Keppens and Goedbloed (2000) used only the poloidal ( $r$  and  $\theta$ ) components of both quantities. However, the differences between these choices tend to be quite insignificant because both the solar-wind flow and the magnetic field are both mostly radial at the distances where  $r_A$  tends to occur.

Figure 1b shows how the radial locations of the MHD critical points vary as a function of the Parker spiral angle  $\Phi$  between  $\mathbf{u}$  and  $\mathbf{B}$ . For a purely radial flow and field ( $\Phi = 0$ ), the slow-mode magnetosonic critical point is just the classical transonic critical point, and the Alfvén and fast-mode critical points coincide with one another at the point where  $u_r = V_A$ . However, the Weber and Davis (1967) model provides a unique solution for  $\Phi$  as a function of radial distance, which is illustrated in Figure 1b and given by

$$\tan \Phi = \frac{B_\phi}{B_r} = \frac{u_\phi - \Omega r \sin \theta}{u_r}. \quad (5)$$

In the high-speed solar-wind model shown here, the field lines are still mostly radial at the Alfvén radius; i.e.  $|\Phi| \approx 2^\circ$  at  $r_A$ , and at that value the fast-mode critical point is only about  $0.007 R_\odot$  ahead of the Alfvén point.

Figure 1b also illustrates the location of the radial distance at which the plasma  $\beta$  ratio approximately equals unity. Here, we apply the definition  $\beta = c_s^2/V_A^2$ , which is a version used frequently in collisionless plasma theory. Defining the adiabatic sound speed as  $c_s$ , this expression for  $\beta$  differs by only a factor of 1.2 from the MHD definition (the ratio of total gas pressure to magnetic pressure) when the adiabatic exponent  $\gamma = 5/3$ . For high-speed solar-wind models like the one shown here, the  $\beta = 1$  radius occurs well above the other critical points. However, some slow-wind streams may experience additional crossings of  $\beta = 1$  near cusp-like null points at the tips of helmet streamers (see Section 2.4). DeForest et al. (2016) suggested that the heliospheric  $\beta = 1$  radius is where

large-scale turbulent plasma features undergo a major transition in geometric aspect ratio. Specifically, below this point they take the form of magnetic-field-aligned rays or striations, and above this point they become more isotropic cloud-like “floculations” unconstrained by the magnetic field.

There are a number of other factors that can affect the locations and properties of the critical points. As mentioned above, waves and turbulence exert a ponderomotive force (“wave pressure”) that affects the location and speed of the Parker critical point (Alazraki and Couturier, 1971; Belcher, 1971; Jacques, 1977; Isenberg and Hollweg, 1982). The existence of super-radial expansion of the magnetic-field lines can give rise to the existence of multiple potential locations of each critical point (Kopp and Holzer, 1976), and only a global examination of the boundary conditions (i.e. what happens as  $r \rightarrow \infty$ ) determines which ones are actual critical points. Although Weber and Davis (1967) assumed a spherically expanding solar wind, their expression for  $u_\phi$  remains valid even with super-radially expanding field lines. Note, however, that the detailed form of Equation 3 changes when one takes account of additional ion species – e.g.  $\alpha$  particles – that flow at different speeds than the background proton–electron plasma (Li and Li, 2006).

## 2.2. Angular Momentum Transport

The solar wind is primarily a source of mass loss for the Sun. On average, its magnitude is  $|dM_\odot/dt| = |\dot{M}| \approx 10^9 \text{ kg s}^{-1}$ , or about  $3 \times 10^{-14} M_\odot \text{ yr}^{-1}$  (see, e.g. Vidotto, 2021). However, because the Sun is rotating, the solar wind is also associated with a continuous loss of angular momentum, which causes the Sun to spin down over time. If the solar wind were released from the Sun’s surface and immediately began to conserve angular momentum (i.e. if  $u_\phi \propto 1/r$ ), the rate of solar angular momentum loss would be

$$\frac{dJ}{dt} = \frac{2}{3} \dot{M} \Omega R_\odot^2 , \quad (6)$$

where the factor of  $2/3$  assumes a spherically symmetric outflow (see Matt and Pudritz, 2005). However, Weber and Davis (1967) showed that a magnetized solar wind increases the “torque lever arm” such that the total rate of angular momentum loss is instead given by

$$\frac{dJ}{dt} = \frac{2}{3} \dot{M} \Omega r_A^2 . \quad (7)$$

Thus, since  $(r_A/R_\odot)^2 \approx 100$ , this leads to several orders of magnitude more rotational wind braking than was suspected to exist originally. Note that the appearance of  $r_A^2$  in Equation 7 sometimes leads to the misconception that the plasma remains rigidly rotating up to the Alfvén radius. The plot of  $u_\phi$  in Figure 1a indicates that this is not the case. In fact, most of the increased angular momentum transport in the Weber and Davis (1967) model is associated not with the rotating plasma, but with Poynting stresses associated with  $B_\phi$ .

The present-day rate of rotational spindown for the Sun has been estimated in various ways. Astronomers have measured rotation frequencies  $\Omega$  for solar-type

stars of a range of ages  $t$ , and there seems to exist a power-law trend of  $\Omega \propto t^{-1/2}$  that persists over billions of years (Skumanich, 1972; Barnes, 2007). This relationship would be the natural result of Equation 7 if  $r_A \propto B \propto \Omega$  and both  $\dot{M}$  and the Sun’s moment of inertia  $I$  remained constant over time; i.e.  $d\Omega/dt \propto -\Omega^3$  (Durney and Stenflo, 1972; Vidotto, 2021). More direct attempts to measure  $dJ/dt$  from combinations of in-situ plasma and magnetic-field data (Pizzo et al., 1983; Li, 1999; Finley et al., 2019; Verscharen et al., 2021b; Finley and Brun, 2023) have yielded results in adequate – but still not precise – agreement with the basic theory. Usmanov et al. (2018) used 3D simulations to model  $dJ/dt$  and showed that the presence of turbulence can also affect the total loss of angular momentum. In addition, Tasnim et al. (2018) found that the near-Sun boundary conditions used in simulations can have a strong impact on the resulting behavior of angular-momentum loss in the heliosphere.

If the Sun is spinning down in a manner consistent with the Skumanich (1972) scaling law [ $\Omega \propto t^{-1/2}$ ], this would imply a rate of period increase of roughly 0.02 seconds per century. Such a change is currently unobservable, but it should be noted that somewhat more rapid changes are observed for pulsars (e.g. Harding, 2013) and at least one main-sequence star (Townsend et al., 2010). For the latter – the magnetic B2-type star  $\sigma$  Ori E – the rate of period increase has been found to be approximately 8 seconds per century, which appears to be consistent with the models of rotational wind braking described above. When considering other stars with a range of magnetic-field strengths, wind mass-loss rates, and rotation rates, there arises an interesting “zoo” of dynamical phenomena that includes shocked wind-fed disks, rigidly rotating stellar magnetospheres, and stochastic competition between plasma infall and centrifugal breakout (see, e.g. Owocki, 2009; ud-Doula, 2017).

### 2.3. Importance to Waves and Turbulence

The Alfvén radius is an important internal boundary condition for models of MHD fluctuations in the solar wind. For example, the simplest models of linear Alfvén-wave evolution along radial field lines often show a local maximum in the wave velocity amplitude in the vicinity of  $r_A$ . Such models of WKB wave action conservation (whose derivation does not require the use of the actual Wentzel–Kramers–Brillouin approximation; see, e.g. Bretherton and Garrett, 1968; Jacques, 1977) find that, in the absence of dissipation, the wave energy flux  $F = \rho v_{\perp}^2 V_A$  should behave as

$$F \propto \frac{B}{1 + M_A^2}. \quad (8)$$

Since the quantity  $\rho M_A^2$  should also be constant along field lines, the transverse velocity amplitude of the waves [ $v_{\perp}$ ] is given by

$$v_{\perp} \propto \rho^{-1/4} \left( 1 + \frac{\rho_A}{\rho} \right)^{-1/2} \quad (9)$$



where  $\rho_A$  is the plasma density at  $r_A$ . Thus, because  $\rho$  is monotonically decreasing with increasing  $r$ ,  $v_\perp$  increases with  $r$  below the Alfvén point (i.e.  $v_\perp \propto \rho^{-1/4}$  for  $\rho \gg \rho_A$ ). The velocity amplitude reaches a local maximum exactly at the Alfvén point, and then it decreases above it, ultimately scaling as  $v_\perp \propto \rho^{+1/4}$  when  $\rho \ll \rho_A$ .

Plasma properties at  $r_A$  are also required when computing global models of non-WKB wave reflection (Heinemann and Olbert, 1980). In an inhomogeneous corona and heliosphere, some fraction of the energy in outgoing waves may be reflected gradually and turned into inward-propagating waves. The Alfvén radius is a singular point of the non-WKB transport equations (see also Barkhudarov, 1991; Velli, 1993; MacGregor and Charbonneau, 1994; Cranmer, 2010). Specifically, the ratio of inward to outward velocity amplitudes at  $r = r_A$ , expressed in terms of inward  $[Z_-]$  and outward  $[Z_+]$  Elsasser (1950) amplitudes, is found via another application of L’Hôpital’s rule,

$$\frac{Z_-}{Z_+} = \frac{|dV_A/dr|}{\sqrt{\omega^2 + [(du/dr) - (dV_A/dr)]^2}}, \quad (10)$$

where  $\omega$  is the wave’s angular frequency and the derivatives are evaluated at  $r_A$ . For  $r > r_A$ , the inward propagating Alfvén waves cannot travel all the way back down to the Sun. However, they can still interact with the outward waves and undergo nonlinear “wave packet collisions” that develop into MHD turbulence and heat the plasma (e.g. Iroshnikov, 1963; Kraichnan, 1965; Hossain et al., 1995). The analysis of non-WKB reflection in the presence of a strongly turbulent cascade also requires treating the Alfvén radius as a singular point (Dmitruk et al., 2002; Chandran and Hollweg, 2009; Chandran and Perez, 2019).

The analysis of turbulent fluctuations measured in-situ can be greatly complicated when the measurement probes approach the Alfvén radius. Further out in the heliosphere (where  $u \gg V_A$ ), it is common to see straightforward applications of Taylor’s (1938) hypothesis of frozen-in fluctuations. This hypothesis assumes that waves and turbulent eddies are essentially static in a reference frame that advects past the spacecraft with the solar-wind velocity  $\mathbf{u}$ . In other words, an observed frequency  $\omega$  in the spacecraft frame is assumed to be equivalent to  $\mathbf{u} \cdot \mathbf{k}$ , where  $\mathbf{k}$  is a wavenumber intrinsic to the propagating fluctuation. However, when a spacecraft approaches the vicinity of the Alfvén radius, the solar-wind velocity is no longer the dominant source of motion. Thus, modifications to Taylor’s hypothesis need to be made (see, e.g. Matthaeus, 1997; Klein et al., 2015; Bourouaine and Perez, 2018; Zank et al., 2022). The study of heliospheric turbulence close to the Sun is still an active field of research, and there have been theoretical predictions of both depletions (Adhikari et al., 2019) and enhancements (Ruffolo et al., 2020) of the fluctuation amplitudes in the vicinity of the Alfvén surface.

#### 2.4. Topological Boundary Between Open and Closed Fields

Once magnetic field lines extend above  $r_A$ , they are unable to propagate information along MHD characteristics back down to the Sun. Thus, it is likely to be

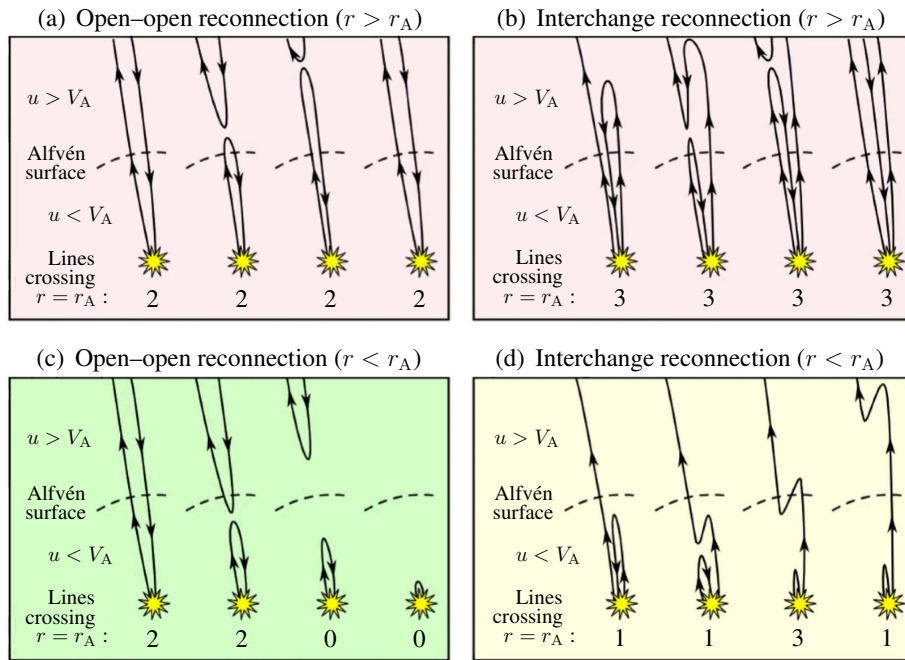


**Figure 2.** Temporal dependence of field lines crossing the Alfvén surface for various kinds of magnetic reconnection.

quite rare to find closed magnetic loops that reach up to the Alfvén radius or beyond. Essentially,  $r_A$  can be considered to be a “source surface” of heliospheric magnetic flux (e.g. Zhao and Hoeksema, 2010). It should be noted that, in the actual time-dependent heliosphere, there are often closed field lines encountered at distances far above  $r_A$  (i.e. detected with double-beamed electron strahls), but these tend to be associated with coronal mass ejection (CME) flux ropes, not parts of the ambient solar wind (Gosling et al., 1987; Shodhan et al., 2000; Smith et al., 2013). Nevertheless, if magnetic reconnection occurs in the outer corona, it may be possible to trace the number of field lines that cross the Alfvén surface, over time, and this number will vary in different ways depending on whether the reconnection occurs above or below  $r_A$ . Figure 2 shows a set of four possibilities, each depending on the type of reconnection and where it occurs (see also Crooker et al., 2002; Schwadron et al., 2010; DeForest et al., 2012).

Near the solar surface, the coronal magnetic field often obeys an approximately force-free configuration ( $\mathbf{J} \times \mathbf{B} \approx 0$ ) that is satisfied by a potential field ( $\mathbf{J} \propto \nabla \times \mathbf{B} = 0$ , so  $\mathbf{B} = -\nabla\Psi$ ) in much of the volume outside filaments and active regions. The scalar potential  $\Psi$  satisfies Laplace’s equation, so it can be expressed as a sum of multipolar spherical harmonics with amplitudes specified by the photospheric lower boundary. However, the acceleration of the solar wind produces MHD forces that stretch open the field lines and cause them to depart from the standard closed shapes (dipole, quadrupole, octupole, and so on). This stretching is often modeled approximately using a radial source-surface boundary condition at  $R_{ss} \approx 2.5 R_\odot$  (Altschuler and Newkirk, 1969; Schatten et al., 1969)

or the entire set of MHD equations is solved numerically (see, e.g. Pneuman and Kopp, 1971; Suess et al., 1999; Gombosi et al., 2018; Usmanov et al., 2018).

A consistent feature of both MHD simulations and observations (from, e.g. the shapes of field lines inferred from visible-light emission seen during total eclipses) is that closed coronal loops do not typically extend all the way up to the Alfvén surface. Although the largest “helmet streamers” can be seen to stretch out to at least 10 to 15  $R_\odot$  (see Annie Maunder’s historical photo reproduced by Dalla and Fletcher 2016), the magnetically closed loop-like features do not appear to extend past radii of 3 to 4  $R_\odot$  (Riley et al., 2006; Mackay and Yeates, 2012). However, one may have expected to find the upper bound of the closed magnetic field to be more like  $r_A$  itself, i.e. radial distances of about 10 to 20  $R_\odot$  (see Section 3). This discrepancy has not been discussed extensively, although Owocki (2009) associated it with the prevalence of high-order multipole components of the field that drop off with  $r$  more rapidly than the dominant dipole component. Also, in some MHD models of streamers (e.g. Keppens and Goedbloed, 2000), the solar wind right above the cusp passes through an Alfvén point at a height even *lower* than Parker’s sonic point. The reduction in  $V_A$  near the cusp’s null point gives the solar wind’s total pressure (gas and ram) the chance to substantially distort the field lines, and even the plasma- $\beta$  ratio can exceed unity in that region (Li, 1999; Lloveras et al., 2017).

Figure 3 illustrates these issues by highlighting the difference between the magnetic pressure associated with  $B_r$  and the magnetic pressure associated with the other (transverse or horizontal) components of the field (see also Vázquez et al., 2003; Réville and Brun, 2017). For these plots, representative curves for the gas and ram pressure were computed using the same example model shown in Figure 1. However, the details of the magnetic pressure come from numerical models computed by the Magnetohydrodynamics Around a Sphere (MAS) code (see, e.g. Linker et al., 1999) and made available by the MHDweb project ([www.predsci.com/mhdweb](http://www.predsci.com/mhdweb)). The photospheric boundary conditions were obtained from Carrington Rotation (CR) 2058, from June–July 2007, with synoptic magnetogram data from the *Solar and Heliospheric Observatory* (SOHO) *Michelson Doppler Imager* (MDI; Scherrer et al., 1995). The magnetic pressures in the corona were extracted at all latitudes and longitudes, with only statistical medians and standard-deviation ranges shown in the plots.

In the low- $\beta$  corona, flows parallel to the field act as “beads on a string” and do not feel significant Lorentz forces. Thus, Figure 3b shows that the height where the ram pressure balances the radial magnetic pressure occurs at  $r_A \approx 10 R_\odot$ , as expected. However, the shapes of the loops and streamers depend more on the force balance perpendicular to  $\mathbf{B}$ , and Figure 3c shows that the associated transverse magnetic pressure is overcome by both gas and ram pressure at lower heights of order 2 to 3  $R_\odot$ . Thus, it is this range of heights that seems to be most naturally associated with the cusps of the largest streamers. As noted by Owocki (2009), the transverse components of the magnetic field in the corona are dominated more by higher-order (quadrupole and octupole) components of the global field, whose strength drops off more rapidly than the dipole component. Thus, the upper limit of closed-loop heights seems to be associated with the same general processes that set the Alfvén surface, but this upper limit does not coincide with  $r_A$  itself.

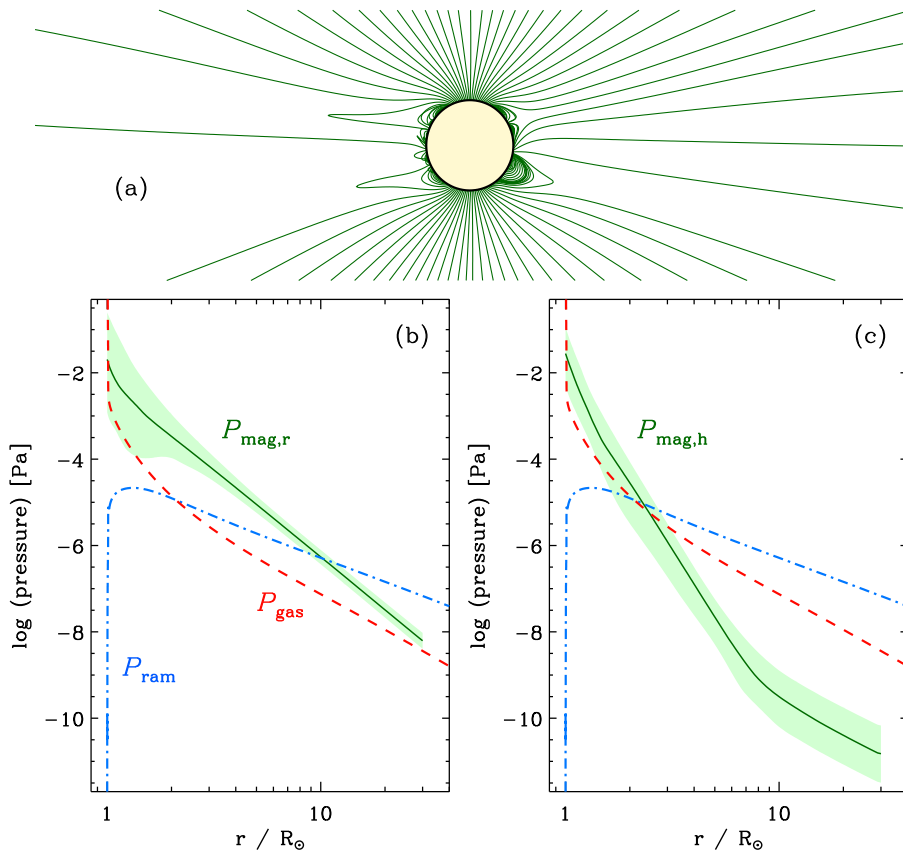


**Figure 3.** (a) Magnetic field lines traced from a time-steady solution of the polytropic MHD conservation equations for Carrington Rotation (CR) 2058. (b) Comparison of radial dependences of time-steady gas pressure (red dashed curve) and ram pressure ( $P_{\text{ram}} = \rho u_r^2/2$ , blue dot-dashed curve) from Figure 1, and radial magnetic pressure extracted from the simulation (median: dark green solid curve,  $\pm 1\sigma$  bounds: light green region). (c) Same as panel (b), but with transverse magnetic pressure.

### 3. Locations of the Alfvén Surface

Having now summarized several ways that the Alfvén surface is important for our physical understanding of the corona and solar wind, the next practical question to ask is: Where is it? Below we summarize quantitative estimates of  $r_A$  from model-based predictions (Section 3.1), in-situ measurements (Section 3.2), and coronagraphic imaging (Section 3.3).

#### 3.1. Corona/Heliosphere Simulations

The first numerical model that incorporated the Alfvén surface was that of Weber and Davis (1967), and their default set of in-ecliptic parameters provided a value of  $r_A = 24.3 R_{\odot}$ . They also noted that the expected range of Alfvén

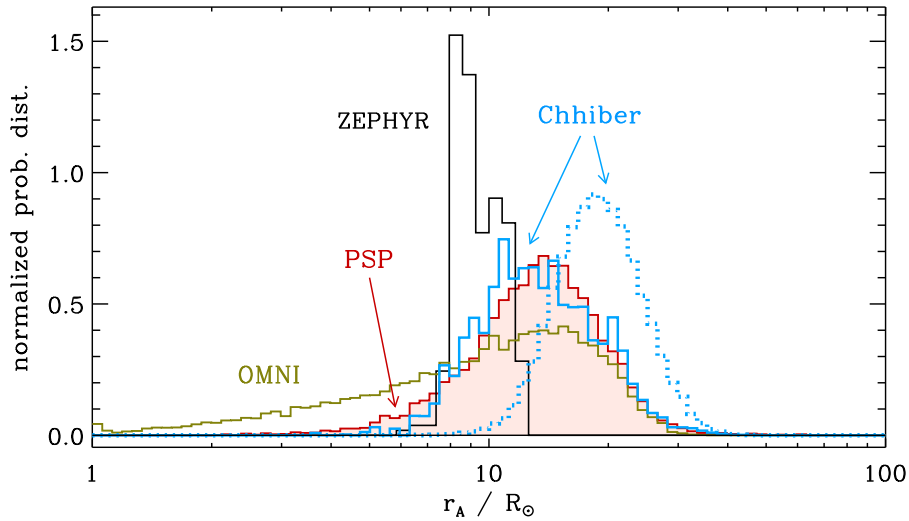


**Figure 4.** Comparison of independent estimates of Alfvén radii, expressed as probability-density histograms. Model results include ZEPHYR (*solid black curve*) and 3D simulations from Chhiber et al. (2022) (in-ecliptic: *solid blue curve*, all latitudes: *dotted blue curve*). Observationally derived radii include those from the OMNI database at 1 AU (*olive curve*) and from PSP (*red curve*). See text for details.

radii – corresponding to the observed variation of solar-wind properties at 1 AU – would be more like  $r_A \approx 15$  to  $50 R_\odot$ . Additional one-dimensional models of coronal heating and solar-wind acceleration have been computed with the ZEPHYR code. Figure 1 shows one specific model of this kind (for polar magnetic field lines rooted in a coronal hole at solar minimum), and Figure 4 shows a histogram of  $r_A$ -values constructed from 319 independent ZEPHYR models: 30 from the polar coronal hole, equatorial helmet streamer, and active region models of Cranmer et al. (2007), and 289 from a high-resolution study of open field lines connected to a diffuse quiet-Sun region, by Cranmer et al. (2013). For these models,  $r_A$  clusters rather tightly around a median value of  $9.16 R_\odot$ , with a standard deviation of only  $1.24 R_\odot$ .

There have been a number of multi-dimensional global simulations that track the variability of  $r_A$  as a function of longitude, latitude, and solar-cycle activity (Pneuman and Kopp, 1971; Keppens and Goedbloed, 2000; Matt and Pudritz, 2008; Cohen et al., 2009; Pinto et al., 2011; Cohen, 2015; Chhiber et al., 2019). The shape of the Alfvén surface follows the large-scale magnetic polarity of the corona, often with local maxima in  $r_A$  occurring near the centers of large polar coronal holes, and local minima occurring at the tops of helmet streamers.

In order to better model the stochastic “frothiness” of the Alfvén zone as realistically as possible, Chhiber et al. (2022) included realizations of turbulent fluctuations in a 3D simulation. In this model, there arise intermixed regions of sub-Alfvénic and super-Alfvénic flow, with one radial ray passing through multiple transitions where  $u = V_A$ . Histograms of values of  $r_A$  can be computed by taking derivatives of cumulative distributions similar to the ones shown in Figure 5 of Chhiber et al. (2022). Figure 4 shows that when all latitudes and

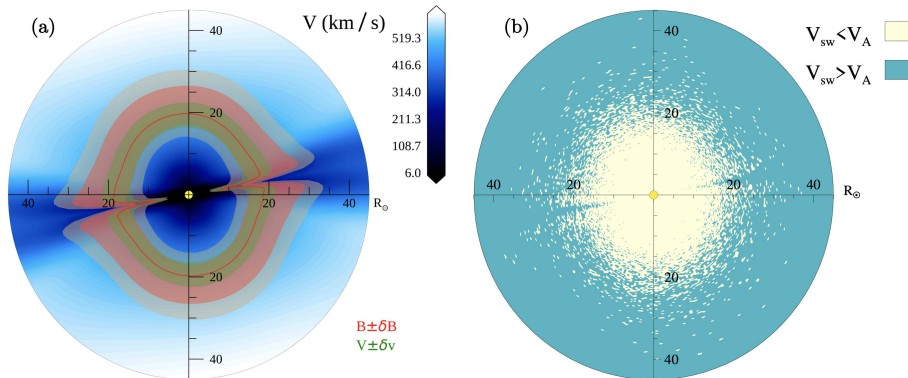


**Figure 5.** An example meridional plane cutting through one of the 3D simulations produced by Chhiber et al. (2022), showing: (a) radial outflow speed (blue to white), overplotted with the mean shape of the Alfvén surface (red solid curve) and ranges of locations over which the Alfvén surface occur over the simulation run when taking into account magnetic fluctuations (light red region) or velocity fluctuations (light green region). (b) Snapshot of the “frothy” separation between sub-Alfvénic (beige) and super-Alfvénic (teal) regions.

longitudes are included, the distribution of Alfvén radii has a substantially higher median value ( $20.1 R_{\odot}$ ) than do the ZEPHYR models. However, when only simulation data for  $\pm 4^{\circ}$  of latitude above and below the ecliptic plane were chosen – specifically for a model that reproduces CR 2215 – the median value of  $r_A$  is lower ( $15.1 R_{\odot}$ ) and in better agreement with the observationally inferred values discussed in more detail below. Figure 5 illustrates these simulations, and Chhiber et al. (2022) discuss further how these patchy structures may be important for driving the largest energy-containing scales of MHD turbulence in the solar wind.

### 3.2. In Situ Extrapolations and Detections

There have been quite a few studies of in-situ spacecraft data that involved extrapolating radial trends from traditionally observed distances ( $r > 0.3$  AU, prior to PSP) inwards to the vicinity of the Alfvén radius. Each of these studies tends to make slightly different assumptions about the radial trends of  $u$  and  $V_A$  – and also different assumptions about which conservation laws are used in the extrapolation process – but they often seem to converge on values for  $r_A$  between about 10 and  $40 R_{\odot}$  (see, e.g. Marsch and Richter, 1984; Exarhos and Moussas, 2000; Katsikas et al., 2010; Goelzer et al., 2014; Tasnim and Cairns, 2016; Tasnim et al., 2018; Kasper and Klein, 2019; Liu et al., 2021; Verscharen et al., 2021a). More recently, combinations of in-situ and remote-sensing data have been used to put additional constraints on the most likely values of  $r_A$  (Wexler et al., 2021; Telloni et al., 2021), and these methods often point to a lower range of about 8 to  $20 R_{\odot}$ .

Perhaps the most straightforward of these extrapolation methods combines the assumption of a constant solar-wind speed, mass-flux conservation far from the Sun ( $\rho \propto r^{-2}$ ) and magnetic-flux conservation far from the Sun ( $B_r \propto r^{-2}$ )

to find that one then expects the Alfvénic Mach number to increase with radial distance as  $M_A \propto r$ . Thus, measuring  $M_A \gg 1$  in interplanetary space provides an anchor-point to extrapolate linearly back to the point where this quantity is equal to unity. Cranmer et al. (2021) showed how this method can be modified to account for the small amount of radial acceleration in the solar-wind speed between  $r_A$  and the in-situ measurement point.

Figure 4 shows our attempt to extrapolate to  $r_A$  using 11 years of in-ecliptic OMNI ([omniweb.gsfc.nasa.gov](https://omniweb.gsfc.nasa.gov)) data taken at 1 AU (King and Papitashvili, 2005) from 2008 to 2018. The extrapolation method is discussed in more detail by Cranmer et al. (2021). CMEs and gaps in the OMNI database were removed, the former using criteria given by Xu and Borovsky (2015), and mean values of the solar-wind parameters were taken using two-hour bins. Note that Cranmer et al. (2021) gave results for only the high-speed solar wind, but the OMNI histogram shown in Figure 4 accounts for all speeds. The resulting distribution of values of  $r_A$  is highly skewed, with a modal maximum at  $15.4 R_\odot$  and a median at  $10.9 R_\odot$ .

Of course, now that the PSP spacecraft has repeatedly crossed into the sub-Alfvénic heliosphere (see, e.g. Kasper et al., 2021; Bandyopadhyay et al., 2022; Zhang et al., 2022; Zhao et al., 2022; Liu et al., 2023), the extrapolation techniques described above can be tested and validated, at least statistically. Figure 6a shows preliminary PSP data for the Alfvénic Mach number  $M_A$  versus heliocentric distance. We computed this quantity as the ratio of  $u_r$  to the total Alfvén speed  $V_A$  (evaluated with the magnitude  $B$ ). To obtain these parameters, we began with one-hour-averaged merged data, produced as a part of NASA’s Coordinated Heliospheric Observations (COHO), that combines Level-3 proton data from the *Solar Probe Cup* (SPC: Case et al., 2020), a component of the *Solar Wind Electrons Alphas and Protons* (SWEAP) suite (Kasper et al., 2016), with Level-2 fluxgate magnetometer data from the FIELDS suite (Bale et al., 2016). Because these data were not always available for the most recent PSP perihelia, we followed Bandyopadhyay et al. (2022) by also incorporating additional proton radial velocity and density data from the SWEAP *Solar Probe Analyzer-Ion* (SPAN-I), with data rejected if any of the SPAN-I quality-flag bits 0, 2, 3, 8, 10, or 11 were set. Also, we incorporated additional plasma density data (with  $n_p = n_e/1.1$ ) from quasi-thermal noise measurements with the FIELDS *Radio Frequency Spectrometer* (RFS: Pulupa et al., 2017) and additional Level-2 fluxgate magnetometer data. Data provided at higher resolution were binned into one-hour averages and used only when the the COHO merged data were unavailable.

We applied the OMNI extrapolation method discussed above to our PSP dataset. An extra step in the analysis was added to account for measurements not at 1 AU, but the same basic algorithm from Cranmer et al. (2021) remained in use. Figure 6b plots these extrapolated values of  $r_A$  versus the radial distance of PSP at the time of each measurement. Note that there is no dominant trend in these derived values as a function of heliocentric distance. The median value for the resulting distribution of  $r_A$  values was  $13.4 R_\odot$ , with a standard deviation of  $5.4 R_\odot$ . Figure 4 shows the corresponding histogram, and its resemblance to that corresponding to the near-ecliptic simulation of Chhiber et al. (2022) is striking.

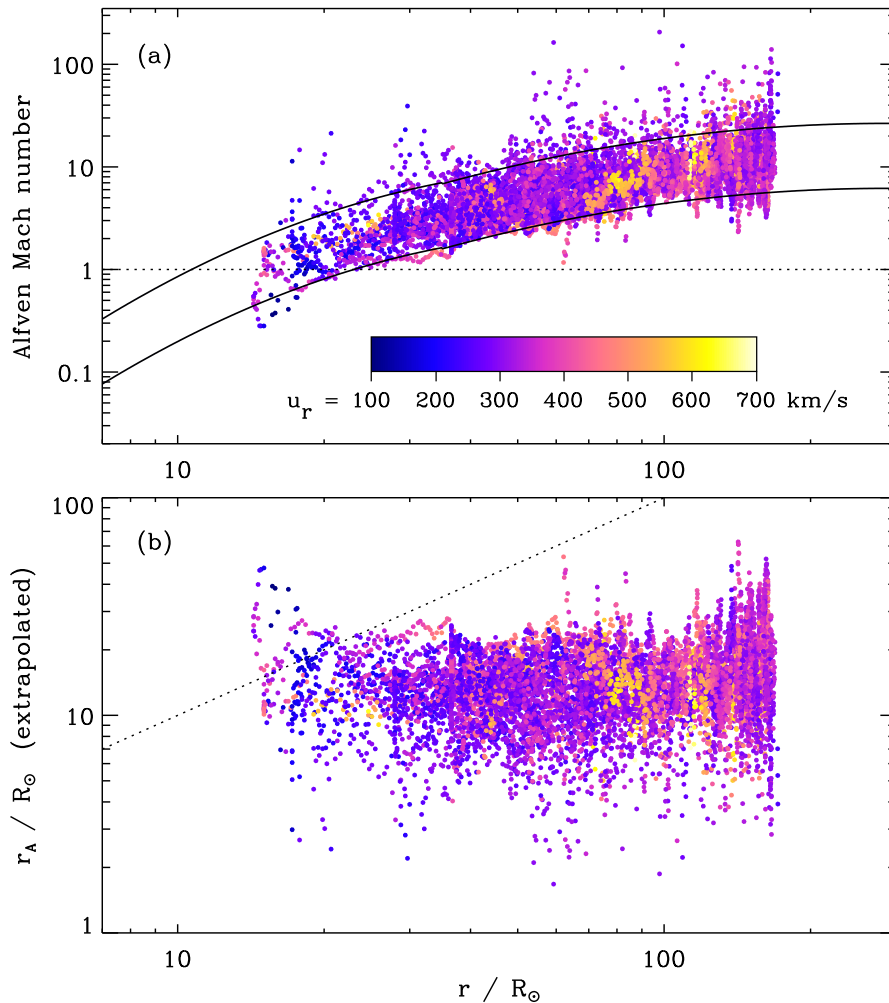


**Figure 6.** Preliminary analysis of PSP data over its first 13 perihelia (October 2018 to October 2022). (a) Alfvénic Mach number  $M_A$  versus heliocentric distance, with measured *solar-wind speeds* shown as symbol color. The solid curves are provided only to indicate the approximate lower and upper bounds of the data. (b) Extrapolated locations of  $r_A$ , plotted versus the heliocentric distance of PSP when each measurement was made. In both panels, the dotted line indicates local crossings of the Alfvén surface.

The PSP histogram also shares a few properties with the histogram computed from OMNI data at 1 AU. For example, the two median values fall within  $\pm 1$  standard deviation of one another, and the upper edges of both distributions are nearly identical. Although it is too early to know for sure, it is likely that data from PSP will end up providing better estimates of  $r_A$  than data taken at 1 AU due to that spacecraft’s more frequent proximity to the Alfvén zone.

Lastly, it is important to note that using in-situ data to extrapolate down to the sub-Alfvénic corona provides benefits beyond just locating the Alfvén sur-



face. Data-driven maps of the vector velocity and magnetic field in the corona can constrain models of turbulence, corotating interaction regions, and suprathermal particle scattering (Tasnim et al., 2018, 2019). Mapping field lines down to the solar surface can help identify the origin sites of different types of fast and slow solar-wind streams (e.g. Luhmann et al., 2002; Liewer et al., 2004). The measurement of cross-field (possibly flux-tube-like) structure in the in-situ data has also been used to speculate about the survival of granular or supergranular scales from the Sun’s surface out to 1 AU (Borovsky, 2008; Tasnim et al., 2018; Bale et al., 2021). These techniques, together with those that map from the corona out to interplanetary space (e.g. Riley and Lionello, 2011; Reiss et al., 2019), are useful in improving forecasts of the time-variable solar wind.

### 3.3. Observations of Coronal Inflows

Coronagraphs and other off-limb imaging instruments have been used for decades to measure outwardly propagating intensity fluctuations that are believed to act as passive tracers (“leaves in the wind”) and thus provide data on the radial acceleration of the solar wind (see, e.g. Sheeley et al., 1997; Abbo et al., 2016). However, there have been rarer detections of plasma flows that go from higher to lower radii over time, and these can be used to put limits on the location of the Alfvén surface. Figure 7 shows how a feature propagating radially – here using the one-dimensional model of Figure 1 – would move in radius versus time, depending on whether it moves with the unperturbed wind speed  $[u_r]$  or on linear Alfvénic characteristics  $[u_r \pm V_A]$ . Note that true inward propagation seems to be possible only for the “minus” Alfvén characteristic, for  $r < r_A$ .

There have been quite a few different types of inflows observed near the Sun. Near the solar surface, there exist supra-arcade downflows in active regions (e.g. Savage et al., 2012) as well as “coronal rain” that propagates down as dense clumps along coronal loops (Antolin et al., 2015; Mason et al., 2019), though many of these flows probably do not connect to the solar wind. At larger heights of about 2 to 6  $R_\odot$ , there are frequent blob-like downflows seen in the vicinity of streamer cusps (Sheeley and Wang, 2014; Sanchez-Diaz et al., 2017; Lynch, 2020). The most distant inflows were found by DeForest et al. (2014), using data from the COR2 coronagraph on the *Solar Terrestrial Relations Observatory* (STEREO-A: Howard et al., 2008). The detection of the weak signals associated with these inflows required the use of customized background subtraction and filtering based on combined spatial and temporal Fourier transforms.

Specifically, for observations made at solar minimum in 2007, DeForest et al. (2014) found inbound features out to at least 12  $R_\odot$  in polar coronal-hole regions, and out to at least 15  $R_\odot$  in the streamer belt. Figure 7 shows an integrated version of the coronal-hole “inflow ridge” measured by DeForest et al. (2014), which was reported originally in terms of radial velocity versus height. These measurements indicated not only substantial deceleration – from speeds of about 80 km s<sup>-1</sup> at 12.4  $R_\odot$  to only about 20 km s<sup>-1</sup> at 7  $R_\odot$  – but also a reduction in magnitude of the parcel’s acceleration that leads to a characteristic “concavity” in the velocity-versus-height diagram. These data appear to confirm that the Alfvén radius must be at a height greater than 12  $R_\odot$  for this component of the solar wind.

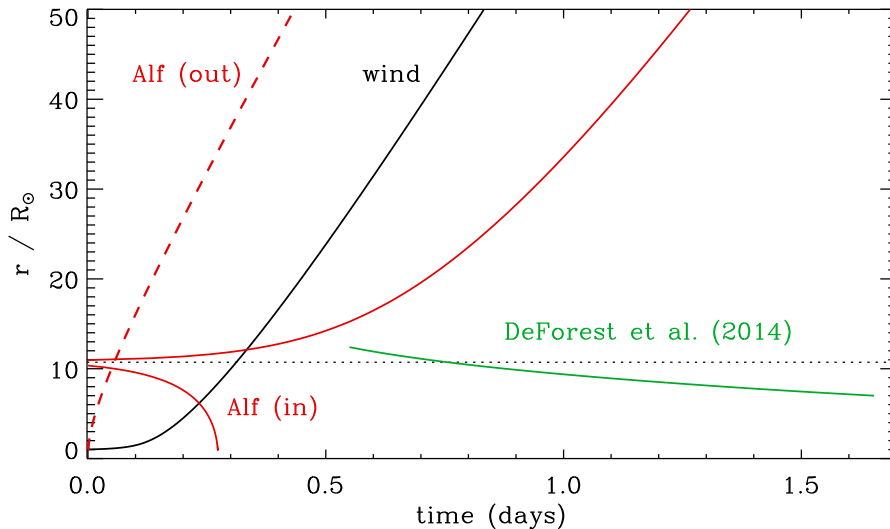


**Figure 7.** Height versus time plots for radial flows that accelerate with the solar wind (black solid curve), with an outward-propagating Alfvén wave (red dashed curve), or with an inward-propagating Alfvén wave (red solid curves). Model parameters are the same as in Figure 1, with  $r_A = 10.7 R_\odot$  (black dotted line). Also shown is a fit to the inward-propagation “ridge” observed in a polar coronal hole by DeForest et al. (2014; green solid curve). For all curves, absolute start times are arbitrary; i.e. any of them can be shifted to the left or right by any amount.

However, Tenerani et al. (2016) noted that the properties of the observed inflow ridge do not match the expected behavior of inwardly propagating Alfvén waves. The latter should accelerate when getting closer to the Sun, not decelerate. Tenerani et al. (2016) also found that other types of linear MHD waves (i.e. obliquely propagating fast or slow magnetosonic waves) may decelerate as they approach the Sun, but they do not agree with the concavity of the measured inflow ridge. One type of model that was found to match the data is one in which a parcel of plasma undergoes a snowplow-like mass enhancement over time, which leads to substantial deceleration as it is entrained into the background flow. Cranmer et al. (2021) produced additional models of snowplow mass-gain in conjunction with hydrodynamic drag forces between the parcel and the ambient solar wind. This kind of model could be consistent with bursty exhausts from coronal sites of magnetic reconnection. Cranmer et al. (2021) also noted that the initial downflow speeds from nonlinear features (e.g. shocks, jets, or shear instabilities) could be somewhat supra-Alfvénic, so they may be able to begin at slightly larger distances than  $r_A$  and still propagate down towards the Sun.

Lastly, it should be noted that a large amount of theoretical speculation has been performed on behalf of a relatively small quantity of existing imaging data in the vicinity of the Alfvén surface. Many more additional examples of inflowing parcel kinematics need to be measured at other locations and times in the solar cycle. Also, it should be noted that Alfvénic fluctuations, by themselves, do not tend to produce the density fluctuations that are most readily observable as variations in off-limb Thomson-scattered intensity. Thus, future theoretical

models need to include a more self-consistent description of either linear or nonlinear compressible features that propagate at speeds similar to  $V_A$  and thus can help probe the location of the Alfvén surface.

#### 4. Discussion: Prospects for PUNCH

The PUNCH mission will image the outer corona and inner heliosphere at radial distances between 6 and 180  $R_\odot$ , with a temporal cadence ranging from four minutes (at  $r < 80 R_\odot$ ) to 35 minutes (for the entire field of view). To measure the flow speeds and accelerations of features in the solar wind, the PUNCH team will use proven methods of spatio-temporal Fourier filtering (DeForest et al., 2014) and a number of flow-tracking algorithms (e.g. Colaninno and Vourlidas, 2006; Chae and Sakurai, 2008; Attié and Innes, 2015). This is being done in collaboration with Working Group 1A of the PUNCH Science Team, whose goal is to map out the spatial and temporal evolution of the “young” solar wind (see, e.g. Attié et al., 2023). PUNCH has been designed with a sensitivity and resolution to enable the accumulation of a huge database of inbound-feature measurements, and these will provide unprecedented information about the variable location of the Alfvén surface.

Although PUNCH will use linear polarization to perform three-dimensional localization of large structures like CMEs (DeForest et al., 2017), it is not yet known to what extent this extra information can be used to improve the tracking of smaller features within the ambient solar wind. Still, it may be the case that synergy between PUNCH and other future missions that include off-limb polarimetry – e.g. the *Association of Spacecraft for Polarimetric and Imaging Investigation of the Corona of the Sun* (ASPIICS: Galano et al., 2018), or the *Coronal Diagnostic Experiment* (CODEX: Newmark et al., 2020) – may provide new perspectives on the use of linear polarization for measuring the properties of the global solar wind.

As mentioned above, PUNCH measures off-limb density inhomogeneities, so it does not directly see incompressible Alfvén waves. However, both slow-mode and fast-mode magnetosonic waves exhibit density oscillations. If, for example, PUNCH observes fast-mode waves propagating radially, these could be used to probe the location of the Alfvén surface because they flow at speeds of roughly  $\pm V_A$  relative to the solar wind (see also Tenerani et al., 2016). The extended corona may also contain nonlinearly steepened features such as shocks, jets, reconnection exhausts, or the end-products of shear instabilities. These can produce observable density perturbations that flow at speeds of order  $V_A$  as well.

The plane-of-sky speeds provided by PUNCH flow-tracking will need to be analyzed in order to estimate the true vector velocities of these features in 3D space. This will be aided by *forward modeling* of these kinds of features (see, e.g. Gibson et al., 2016; Griton et al., 2020; Gilly et al., 2021; Moraes Filho et al., 2022), together with the development of robust uncertainty bounds on this kind of 3D localization. The properties of the measured density inhomogeneities will also need to be correlated with the ambient properties of the solar wind and the

global magnetic geometry of the corona. Specifically, PUNCH data will provide many examples of both: i) the direct measurement of  $V_A$  at  $r_A$ , from knowing the bulk solar-wind speed there, and ii) maps of the plane-of-sky shape of the Alfvén surface. These can help discriminate between competing solar-wind models and provide large-scale context for future multi-messenger campaigns with PSP and Solar Orbiter (see, e.g. Martínez Pillet et al., 2023).

It will be interesting to learn whether or not all measured inflow tracks will have the same speed and acceleration trends (i.e. concavity) as the one set of events studied by DeForest et al. (2014) and Tenerani et al. (2016). It is possible that the one inbound feature measured by COR2 was the “tip of the iceberg” and thus is not representative of the broader population of lower-contrast features to be seen by PUNCH. Because these other features may have weaker density fluctuations, they may not undergo substantial amounts of snowplow-like mass-gain. Thus, they may have speeds more representative of linear MHD waves. We expect to explore trends in the inflow dynamics as a function of the relative intensity enhancements (i.e. relative density enhancements) of blobs, which will help validate the physics included in models that include mass-gain and drag forces (e.g. Cranmer et al., 2021).

It is also very likely that the region around the Alfvén radius is highly turbulent, so there may exist multiple crossings in a frothy “Alfvén zone” (see also DeForest et al., 2018; Chhiber et al., 2022). One implication of this, which PUNCH may be very well-suited to observe, is that individual blobs would undergo stochastic (random-walk-type) deflections when near the Alfvén zone. Thus, they would propagate alternately in and out for a while before heading decidedly either towards the Sun or the outer heliosphere. Figure 8 shows the result of a simple one-dimensional simulation that accounts for this stochasticity. A continuous Kolmogorov-type spectrum of fluctuations (i.e. power proportional to  $f^{-5/3}$ ) was sampled at 100 discrete frequencies  $f$  sampled between  $10^{-4}$  and 1 Hz, with random phases. Then, one independently constructed time-series was imposed on the background wind speed  $u_r(r)$ , and another was imposed on the Alfvén speed  $[V_A]$ , each with the same renormalized relative amplitude, as shown in Figure 8a.

Because models of non-WKB wave reflection usually show a preponderance for outward waves in the corona, our simulated fluctuations were assumed to propagate along outward Alfvén characteristics (i.e. at  $u_r + V_A$ ) over time. However, we then chose to focus on the temporal evolution of parcels that attempt to approach the Sun on inward characteristics  $[u_r - V_A]$ . Due to the in/out motion of multiple Alfvén radii in this model, it becomes possible for some parcels that begin at  $r < r_A$  to eventually escape, and for some parcels that begin at  $r > r_A$  to eventually flow downwards and reach the Sun. Figure 8b illustrates this by plotting histograms of a statistical “escape probability” constructed from three sets of 10,000 random trials. The three sets had different relative amplitudes for the imposed fluctuations, and one can see that as this amplitude approaches zero, the escape probability approaches a step function that is zero for  $r < r_A$  and one for  $r > r_A$ . PSP observations indicate that these relative amplitudes are reasonable for the radii shown here (Chhiber, 2022).

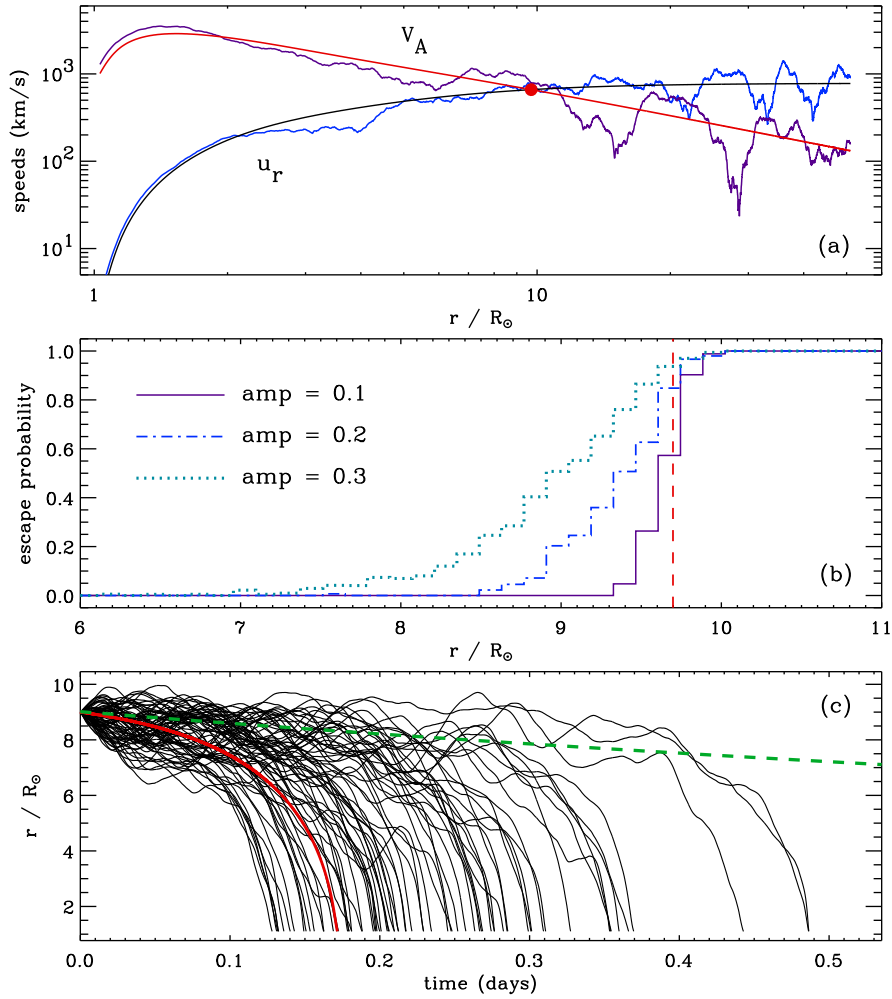


**Figure 8.** Preliminary model of stochastic motions in the solar wind. (a) Example snapshot of  $u_r$  and  $V_A$ , both with no turbulence (*black and red curves*) and with turbulence included at a fractional amplitude of 0.3 times the time-steady values (*blue and violet curves*). (b) Escape probability of a parcel that flows with local radial speed ( $u_r - V_A$ ), averaged over 10,000 trials for each value of turbulence amplitude. The time-steady value of  $r_A$  is shown with a *dashed red line*. (c) Downward trajectories that include turbulence at an amplitude of 0.3 (*black curves*) and one that does not (*red curve*), compared with observed COR2 inflow data (*green dashed curve*).

Lastly, Figure 8c shows a collection of inflow trajectories for parcels that started at  $r = 9 R_\odot$  (slightly below the time-steady Alfvén radius, which for this model was  $9.7 R_\odot$ ) and eventually flowed down to the Sun. A parcel flowing inwards along unperturbed inward Alfvén characteristics (i.e. with no “froth”) would reach the Sun in only about 0.17 days, but the distribution of perturbed parcels has a longer mean flow time. These perturbed parcels become trapped in the trans-Alfvénic zone due to being pivoted in the in/out direction multiple

times, and this effectively *decelerates* them. Thus, this effect may help explain the observed inflow trend from DeForest et al. (2014). We anticipate that PUNCH will have the sensitivity, cadence, and spatial resolution to be able to detect these kinds of alternating inflows and outflows for parcels buffeted by turbulence. In fact, if PUNCH can measure the lifetimes, sizes, and relative densities of these parcels, it can put new constraints on models of MHD turbulence in the solar wind.

## 5. Conclusions

The objective of this article has been to review our present-day understanding of the Sun’s Alfvén surface and to look forward to how the PUNCH mission will improve that understanding. This is the goal of Working Group 1C of the PUNCH Science Team, and it connects to the higher-level goal of the mission’s Science Objective 1 (“to understand how coronal structures become the ambient solar wind”). Earlier, we discussed how the flow-tracking activities of Working Group 1A are necessary to provide the measurements of time-dependent flow speeds that can help map the Alfvén surface. In addition, what we learn about the frothy and stochastic Alfvén zone from PUNCH will be also be highly relevant to Working Group 1B, whose goal is to determine how micro-structures and turbulence form and evolve in the solar wind (Viall et al., 2021; Pecora et al., 2023).

Understanding the Alfvén surface associated with a magnetized wind is also relevant for solar systems beyond our own. For example, it is likely that six out of the seven planets orbiting the nearby M-dwarf TRAPPIST-1 spend most of their time inside the star’s sub-Alfvénic zone (Garraffo et al., 2017). This tends to create planetary magnetospheres quite different in character from those seen in our solar system. For example, the motion of close-in exoplanets may disturb the plasma sufficiently to induce strong energy fluxes that go back down to the star (e.g. Saur et al., 2013; Matsakos et al., 2015), producing visible chromospheric starspots (Shkolnik et al., 2008) or bursts of radio emission (Pineda and Villadsen, 2023). There are fascinating opportunities for synergy between studies of our own Alfvén surface, which we can study up close and in detail, and those of other stars, which allow us to sample a much broader range of plasma parameters (Garcia-Sage et al., 2023).

**Acknowledgments** The authors thank Sean Matt, Alex Chasapis, Riddhi Bandyopadhyay, and Dusan Odstrcil for valuable discussions. We are also grateful to the anonymous referee, guest editor, and editor-in-chief, who made many constructive suggestions that have improved this article. The authors acknowledge NASA’s Space Physics Data Facility and COHOWeb for access to the OMNI and PSP data. The National Center for Atmospheric Research is a major facility sponsored by the National Science Foundation under Cooperative Agreement 1852977. *Parker Solar Probe* was designed, built, and is now operated by the Johns Hopkins Applied Physics Laboratory as part of NASA’s Living with a Star (LWS) program (contract NNN06AA01C). Support from the LWS management

and technical team has played a critical role in the success of the *Parker Solar Probe* mission. The authors also thank the FIELDS team (PI: Stuart Bale, UC Berkeley) and the SWEAP team (PI: Justin Kasper, BWX Technologies) for providing data to the archive. This research made extensive use of NASA's Astrophysics Data System (ADS).

**Funding** This work was supported by the National Aeronautics and Space Administration (NASA) via contract 80GSFC18C0014 for the PUNCH Small Explorer mission. Additional support came from NASA via grants 80NSSC20K1319, 80NSSC18K1648, and 80NSSC22K1020, and from the National Science Foundation (NSF) via grant 1613207.

## Declarations

**Conflict of interest** The authors declare that they have no conflicts of interest.

## References

- Abbo, L., Ofman, L., Antiochos, S.K., Hansteen, V.H., Harra, L., Ko, Y.-K., Lapenta, G., Li, B., Riley, P., Strachan, L., von Steiger, R., Wang, Y.-M.: 2016, Slow solar wind: Observations and modeling. *Space Sci. Rev.* **201**, 55. DOI. ADS.
- Adhikari, L., Zank, G.P., Zhao, L.-L.: 2019, Does turbulence turn off at the Alfvén critical surface? *Astrophys. J.* **876**, 26. DOI. ADS.
- Alazraki, G., Couturier, P.: 1971, Solar wind acceleration caused by the gradient of Alfvén wave pressure. *Astron. Astrophys.* **13**, 380. ADS.
- Altschuler, M.D., Newkirk, G.: 1969, Magnetic fields and the structure of the solar corona, I: Methods of calculating coronal fields. *Solar Phys.* **9**, 131. DOI. ADS.
- Antolin, P., Vissers, G., Pereira, T.M.D., Rouppe van der Voort, L., Scullion, E.: 2015, The multithermal and multi-stranded nature of coronal rain. *Astrophys. J.* **806**, 81. DOI. ADS.
- Attié, R., Innes, D.E.: 2015, Magnetic balltracking: Tracking the photospheric magnetic flux. *Astron. Astrophys.* **574**, A106. DOI. ADS.
- Attié, R., Thompson, B.J., Moraes Filho, V., Tremblay, B., Viall, N.M., Gallardo-Lacourt, B., Provornikova, E., Malanushenko, A.: 2023, Mapping solar wind flows with PUNCH. *Solar Phys.*, in preparation.
- Bale, S.D., Goetz, K., Harvey, P.R., Turin, P., Bonnell, J.W., Dudok de Wit, T., Ergun, R.E., MacDowall, R.J., Pulupa, M., Andre, M., Bolton, M., Bougeret, J.-L., Bowen, T.A., Burgess, D., Cattell, C.A., Chandran, B.D.G., Chaston, C.C., Chen, C.H.K., Choi, M.K., Cranmer, S.R., Diaz-Aguado, M., Donakowski, W., Drake, J.F., Farrell, W.M., Ferreau, P., Fermin, J., Fischer, J., Fox, N., Glaser, D., Goldstein, M., Gordon, D., Hanson, E., Harris, S.E., Hayes, L.M., Hinze, J.J., Hollweg, J.V., Horbury, T.S., Howard, R., Hoxie, V., Jannet, G., Karlsson, M., Kasper, J.C., Kellogg, P.J., Kien, M., Klimchuk, J.A., Krasnoselskikh, V.V., Krucker, S., Lynch, J.J., Maksimovic, M., Malaspina, D.M., Marker, S., Martin, P., Martinez-Oliveros, J., McCauley, J., McComas, D.J., McDonald, T., Meyer-Vernet, N., Moncuquet, M., Monson, S.J., Mozer, F.S., Murphy, S.D., Odom, J., Oliverson, R., Olson, J., Parker, E.N., Pankow, D., Phan, T., Quataert, E., Quinn, T., Ruplin, S.W., Salem, C., Seitz, D., Sheppard, D.A., Siy, A., Stevens, K., Summers, D., Szabo, A., Timofeeva, M., Vaivads, A., Velli, M., Yehle, A., Werthimer, D., Wygant, J.R.: 2016, The FIELDS instrument suite for Solar Probe Plus: Measuring the coronal plasma and magnetic field, plasma waves and turbulence, and radio signatures of solar transients. *Space Sci. Rev.* **204**, 49. DOI. ADS.
- Bale, S.D., Horbury, T.S., Velli, M., Desai, M.I., Halekas, J.S., McManus, M.D., Panasenco, O., Badman, S.T., Bowen, T.A., Chandran, B.D.G., Drake, J.F., Kasper, J.C., Laker, R., Mallet, A., Matteini, L., Phan, T.D., Raouafi, N.E., Squire, J., Woodham, L.D., Woolley, T.: 2021, A solar source of Alfvénic magnetic field switchbacks: In situ remnants of magnetic funnels on supergranulation scales. *Astrophys. J.* **923**, 174. DOI. ADS.
- Bandyopadhyay, R., Matthaeus, W.H., McComas, D.J., Chhiber, R., Usmanov, A.V., Huang, J., Livi, R., Larson, D.E., Kasper, J.C., Case, A.W., Stevens, M., Whittlesey, P., Romeo, O.M., Bale, S.D., Bonnell, J.W., Dudok de Wit, T., Goetz, K., Harvey, P.R., MacDowall,

- R.J., Malaspina, D.M., Pulupa, M.: 2022, Sub-Alfvénic solar wind observed by the Parker Solar Probe: Characterization of turbulence, anisotropy, intermittency, and switchback. *Astrophys. J. Lett.* **926**, L1. DOI ADS.
- Barkhudarov, M.R.: 1991, Alfvén waves in stellar winds. *Solar Phys.* **135**, 131. DOI ADS.
- Barnes, S.A.: 2007, Ages for illustrative field stars using gyrochronology: Viability, limitations, and errors. *Astrophys. J.* **669**, 1167. DOI ADS.
- Belcher, J.W.: 1971, Alfvénic wave pressures and the solar wind. *Astrophys. J.* **168**, 509. DOI ADS.
- Belcher, J.W., MacGregor, K.B.: 1976, Magnetic acceleration of winds from solar-type stars. *Astrophys. J.* **210**, 498. DOI ADS.
- Borovsky, J.E.: 2008, Flux tube texture of the solar wind: Strands of the magnetic carpet at 1 AU? *J. Geophys. Res.* **113**, A08110. DOI ADS.
- Bourouaine, S., Perez, J.C.: 2018, On the limitations of Taylor’s hypothesis in Parker Solar Probe’s measurements near the Alfvén critical point. *Astrophys. J. Lett.* **858**, L20. DOI ADS.
- Bretherton, F.P., Garrett, C.J.R.: 1968, Wavetrains in inhomogeneous moving media. *Proc. Roy. Soc. London A* **302**, 529. DOI ADS.
- Case, A.W., Kasper, J.C., Stevens, M.L., Korreck, K.E., Paulson, K., Daigneau, P., Caldwell, D., Freeman, M., Henry, T., Klingensmith, B., Bookbinder, J.A., Robinson, M., Berg, P., Tiu, C., Wright, K.H., Reinhart, M.J., Curtis, D., Ludlam, M., Larson, D., Whittlesey, P., Livi, R., Klein, K.G., Martinović, M.M.: 2020, The Solar Probe Cup on the Parker Solar Probe. *Astrophys. J. Suppl.* **246**, 43. DOI ADS.
- Chae, J., Sakurai, T.: 2008, A test of three optical flow techniques: LCT, DAVE, and NAVE. *Astrophys. J.* **689**, 593. DOI ADS.
- Chandran, B.D.G., Hollweg, J.V.: 2009, Alfvén wave reflection and turbulent heating in the solar wind from 1 solar radius to 1 AU: An analytical treatment. *Astrophys. J.* **707**, 1659. DOI ADS.
- Chandran, B.D.G., Perez, J.C.: 2019, Reflection-driven magnetohydrodynamic turbulence in the solar atmosphere and solar wind. *J. Plasma Phys.* **85**, 905850409. DOI ADS.
- Chhiber, R.: 2022, Anisotropic magnetic turbulence in the inner heliosphere: Radial evolution of distributions observed by Parker Solar Probe. *Astrophys. J.* **939**, 33. DOI ADS.
- Chhiber, R., Matthaeus, W.H., Usmanov, A.V., Bandyopadhyay, R., Goldstein, M.L.: 2022, An extended and fragmented Alfvén zone in the young solar wind. *Mon. Not. Roy. Astron. Soc.* **513**, 159. DOI ADS.
- Chhiber, R., Usmanov, A.V., Matthaeus, W.H., Goldstein, M.L.: 2019, Contextual predictions for the Parker Solar Probe, I: Critical surfaces and regions. *Astrophys. J. Suppl.* **241**, 11. DOI ADS.
- Cohen, O.: 2015, Quantifying the difference between the flux-tube expansion factor at the source surface and at the Alfvén surface using a global MHD model for the solar wind. *Solar Phys.* **290**, 2245. DOI ADS.
- Cohen, O., Drake, J.J., Kashyap, V.L., Gombosi, T.I.: 2009, The effect of magnetic spots on stellar winds and angular momentum loss. *Astrophys. J.* **699**, 1501. DOI ADS.
- Colaninno, R.C., Vourlidas, A.: 2006, Analysis of the velocity field of CMEs using optical flow methods. *Astrophys. J.* **652**, 1747. DOI ADS.
- Cranmer, S.R.: 2010, An efficient approximation of the coronal heating rate for use in global Sun-heliosphere simulations. *Astrophys. J.* **710**, 676. DOI ADS.
- Cranmer, S.R.: 2020, Updated measurements of proton, electron, and oxygen temperatures in the fast solar wind. *Res. Notes Am. Astron. Soc.* **4**, 249. DOI ADS.
- Cranmer, S.R., DeForest, C.E., Gibson, S.E.: 2021, Inward-propagating plasma parcels in the solar corona: Models with aerodynamic drag, ablation, and snowplow accretion. *Astrophys. J.* **913**, 4. DOI ADS.
- Cranmer, S.R., van Ballegoijen, A.A., Edgar, R.J.: 2007, Self-consistent coronal heating and solar wind acceleration from anisotropic magnetohydrodynamic turbulence. *Astrophys. J. Suppl.* **171**, 520. DOI ADS.
- Cranmer, S.R., van Ballegoijen, A.A., Woolsey, L.N.: 2013, Connecting the Sun’s high-resolution magnetic carpet to the turbulent heliosphere. *Astrophys. J.* **767**, 125. DOI ADS.
- Crooker, N.U., Gosling, J.T., Kahler, S.W.: 2002, Reducing heliospheric magnetic flux from coronal mass ejections without disconnection. *J. Geophys. Res.* **107**, 1028. DOI ADS.
- Dalla, S., Fletcher, L.: 2016, A pioneer of solar astronomy. *Astron. Geophys.* **57**, 5.21. DOI ADS.



- DeForest, C.E., de Koning, C.A., Elliott, H.A.: 2017, 3D polarized imaging of coronal mass ejections: Chirality of a CME. *Astrophys. J.* **850**, 130. DOI ADS.
- DeForest, C.E., Howard, T.A., McComas, D.J.: 2012, Disconnecting open solar magnetic flux. *Astrophys. J.* **745**, 36. DOI ADS.
- DeForest, C.E., Howard, T.A., McComas, D.J.: 2014, Inbound waves in the solar corona: A direct indicator of the Alfvén surface location. *Astrophys. J.* **787**, 124. DOI ADS.
- DeForest, C.E., Howard, R.A., Velli, M., Viall, N., Vourlidas, A.: 2018, The highly structured outer solar corona. *Astrophys. J.* **862**, 18. DOI ADS.
- DeForest, C.E., Killough, R., Gibson, S., Henry, A., Case, T., Beasley, M., Laurent, G., Colaninno, R., Waltham, N., PUNCH Science Team: 2022, Polarimeter to Unify the Corona and Heliosphere (PUNCH): Science, status, and path to flight. In: *Proc. 2022 IEEE Aerospace Conference*, 1. DOI ADS.
- DeForest, C.E., Matthaeus, W.H., Viall, N.M., Cranmer, S.R.: 2016, Fading coronal structure and the onset of turbulence in the young solar wind. *Astrophys. J.* **828**, 66. DOI ADS.
- Dmitruk, P., Matthaeus, W.H., Milano, L.J., Oughton, S., Zank, G.P., Mullan, D.J.: 2002, Coronal heating distribution due to low-frequency, wave-driven turbulence. *Astrophys. J.* **575**, 571. DOI ADS.
- Durney, B.R., Stenflo, J.O.: 1972, On stellar activity cycles. *Astrophys. Space Sci.* **15**, 307. DOI ADS.
- Elsasser, W.M.: 1950, The hydromagnetic equations. *Phys. Rev.* **79**, 183. DOI ADS.
- Exarhos, G., Moussas, X.: 2000, An estimation of the shape and temporal variation of the solar wind sonic, Alfvénic, and fast magnetosonic surfaces. *Astron. Astrophys.* **356**, 315. ADS.
- Ferraro, V.C.A.: 1937, The non-uniform rotation of the Sun and its magnetic field. *Mon. Not. Roy. Astron. Soc.* **97**, 458. DOI ADS.
- Finley, A.J., Brun, A.S.: 2023, Accounting for differential rotation in calculations of the Sun's angular momentum-loss rate. *Astron. Astrophys.* **674**, A42. DOI ADS.
- Finley, A.J., Deshmukh, S., Matt, S.P., Owens, M., Wu, C.-J.: 2019, Solar angular momentum loss over the past several millennia. *Astrophys. J.* **883**, 67. DOI ADS.
- Fox, N.J., Velli, M.C., Bale, S.D., Decker, R., Driesman, A., Howard, R.A., Kasper, J.C., Kinnison, J., Kusterer, M., Lario, D., Lockwood, M.K., McComas, D.J., Raouafi, N.E., Szabo, A.: 2016, The Solar Probe Plus mission: Humanity's first visit to our star. *Space Sci. Rev.* **204**, 7. DOI ADS.
- Galano, D., Bemporad, A., Buckley, S., Cernica, I., Dániel, V., Denis, F., de Vos, L., Fineschi, S., Galy, C., Graczyk, R., Horodyska, P., Jacob, J., Jansen, R., Kranitis, N., Kurowski, M., Ladno, M., Ledent, P., Loreggia, D., Melich, R., Mollet, D., Mosdorf, M., Paschalis, A., Peresty, R., Purica, M., Radzik, B., Rataj, M., Rougeot, R., Salvador, L., Thizy, C., Versluys, J., Walczak, T., Zarzycka, A., Zender, J., Zhukov, A.: 2018, Development of ASPIICS: A coronagraph based on Proba-3 formation flying mission. *Proc. SPIE* **10698**, 106982Y. DOI ADS.
- Garcia-Sage, K., Farrish, A.O., Airapetian, V.S., Alexander, D., Cohen, O., Domagal-Goldman, S., Dong, C., Gronoff, G., Halford, A.J., Lazio, J., Luhmann, J.G., Schwieterman, E., Sciola, A., Segura, A., Toffoletto, F., Vievering, J., Ahmed, M.R., Bali, K., Rau, G.: 2023, Star-exoplanet interactions: A growing interdisciplinary field in heliophysics. *Front. Astron. Space Sci.* **10**, 1064076. DOI ADS.
- Garraffo, C., Drake, J.J., Cohen, O., Alvarado-Gómez, J.D., Moschou, S.P.: 2017, The threatening magnetic and plasma environment of the TRAPPIST-1 planets. *Astrophys. J. Lett.* **843**, L33. DOI ADS.
- Gibson, S., Kucera, T., White, S., Dove, J., Fan, Y., Forland, B., Rachmeler, L., Downs, C., Reeves, K.: 2016, FORWARD: A toolset for multiwavelength coronal magnetometry. *Front. Astron. Space Sci.* **3**, 8. DOI ADS.
- Gilly, C.R., Cranmer, S.R., Gibson, S.E.: 2021, STRIA: A new module within FORWARD towards modelling PUNCH datasets. *Bull. Am. Astron. Soc.*, **53**, 2021n6i328p02. ADS.
- Goelzer, M.L., Schwadron, N.A., Smith, C.W.: 2014, An analysis of Alfvén radius based on sunspot number from 1749 to today. *J. Geophys. Res.* **119**, 115. DOI ADS.
- Gombosi, T.I., van der Holst, B., Manchester, W.B., Sokolov, I.V.: 2018, Extended MHD modeling of the steady solar corona and the solar wind. *Liv. Rev. Solar Phys.* **15**, 4. DOI ADS.
- Gosling, J.T., Baker, D.N., Bame, S.J., Feldman, W.C., Zwickl, R.D., Smith, E.J.: 1987, Bidirectional solar wind electron heat flux events. *J. Geophys. Res.* **92**, 8519. DOI ADS.

- Griton, L., Pinto, R.F., Poirier, N., Kouloumvakos, A., Lavarra, M., Rouillard, A.P.: 2020, Coronal bright points as possible sources of density variations in the solar corona. *Astrophys. J.* **893**, 64. DOI. ADS.
- Harding, A. K.: 2013, The neutron star zoo. *Front. Phys.* **8**, 679. DOI. ADS.
- Heinemann, M., Olbert, S.: 1980, Non-WKB Alfvén waves in the solar wind. *J. Geophys. Res.* **85**, 1311. DOI. ADS.
- Hollweg, J.V.: 1970, Collisionless solar wind, I: Constant electron temperature. *J. Geophys. Res.* **75**, 2403. DOI. ADS.
- Holzer, T.E., Leer, E.: 1997, Coronal hole structure and the high-speed solar wind. In: A. Wilson (ed.), *Fifth SOHO Workshop: The Corona and Solar Wind Near Minimum Activity*, 404, ESA, Noordwijk, 65. ADS.
- Hossain, M., Gray, P.C., Pontius, D.H., Matthaeus, W.H., Oughton, S.: 1995, Phenomenology for the decay of energy-containing eddies in homogeneous MHD turbulence. *Phys. Fluids* **7**, 2886. DOI. ADS.
- Howard, R.A., Moses, J.D., Vourlidas, A., Newmark, J.S., Socker, D.G., Plunkett, S.P., Korendyke, C.M., Cook, J.W., Hurley, A., Davila, J.M., Thompson, W.T., St Cyr, O.C., Mentzell, E., Mehalick, K., Lemen, J.R., Wuelser, J.P., Duncan, D.W., Tarbell, T.D., Wolfson, C.J., Moore, A., Harrison, R.A., Waltham, N.R., Lang, J., Davis, C.J., Eyles, C.J., Mapson-Menard, H., Simnett, G.M., Halain, J.P., Defise, J.M., Mazy, E., Rochus, P., Mercier, R., Ravet, M.F., Delmotte, F., Auchere, F., Delaboudiniere, J.P., Bothmer, V., Deutsch, W., Wang, D., Rich, N., Cooper, S., Stephens, V., Maahs, G., Baugh, R., McMullin, D., Carter, T.: 2008, Sun Earth Connection Coronal and Heliospheric Investigation (SECCHI). *Space Sci. Rev.* **136**, 67. DOI. ADS.
- Hundhausen, A.J.: 1972, *Coronal Expansion and Solar Wind*, *Phys. Chem. in Space*, **5**, Springer-Verlag, Berlin. DOI. ADS.
- Iroshnikov, P.S.: 1963, Turbulence of a conducting fluid in a strong magnetic field. *Astron. Zh.* **40**, 742. ADS.
- Isenberg, P.A., Hollweg, J.V.: 1982, Finite amplitude Alfvén waves in a multi-ion plasma: Propagation, acceleration, and heating. *J. Geophys. Res.* **87**, 5023. DOI. ADS.
- Jacques, S.A.: 1977, Momentum and energy transport by waves in the solar atmosphere and solar wind. *Astrophys. J.* **215**, 942. DOI. ADS.
- Kasper, J.C., Abiad, R., Austin, G., Balat-Pichelin, M., Bale, S.D., Belcher, J.W., Berg, P., Bergner, H., Berthomier, M., Bookbinder, J., Brodu, E., Caldwell, D., Case, A.W., Chandran, B.D.G., Cheimets, P., Cirtain, J.W., Cranmer, S.R., Curtis, D.W., Daigneau, P., Dalton, G., Dasgupta, B., DeTomaso, D., Diaz-Aguado, M., Djordjevic, B., Donaskowski, B., Effinger, M., Florinski, V., Fox, N., Freeman, M., Gallagher, D., Gary, S.P., Gauron, T., Gates, R., Goldstein, M., Golub, L., Gordon, D.A., Gurnee, R., Guth, G., Halekas, J., Hatch, K., Heerikuisen, J., Ho, G., Hu, Q., Johnson, G., Jordan, S.P., Korreck, K.E., Larson, D., Lazarus, A.J., Li, G., Livi, R., Ludlam, M., Maksimovic, M., McFadden, J.P., Marchant, W., Maruca, B.A., McComas, D.J., Messina, L., Mercer, T., Park, S., Peddie, A.M., Pogorelov, N., Reinhart, M.J., Richardson, J.D., Robinson, M., Rosen, I., Skoug, R.M., Slagle, A., Steinberg, J.T., Stevens, M.L., Szabo, A., Taylor, E.R., Tiu, C., Turin, P., Velli, M., Webb, G., Whittlesey, P., Wright, K., Wu, S.T., Zank, G.: 2016, Solar Wind Electrons Alphas and Protons (SWEAP) investigation: Design of the solar wind and coronal plasma instrument suite for Solar Probe Plus. *Space Sci. Rev.* **204**, 131. DOI. ADS.
- Kasper, J.C., Klein, K.G.: 2019, Strong preferential ion heating is limited to within the solar Alfvén surface. *Astrophys. J. Lett.* **877**, L35. DOI. ADS.
- Kasper, J.C., Klein, K.G., Lichko, E., Huang, J., Chen, C.H.K., Badman, S.T., Bonnell, J., Whittlesey, P.L., Livi, R., Larson, D., Pulupa, M., Rahmati, A., Stansby, D., Korreck, K.E., Stevens, M., Case, A.W., Bale, S.D., Maksimovic, M., Moncuquet, M., Goetz, K., Halekas, J.S., Malaspina, D., Raouafi, N.E., Szabo, A., MacDowall, R., Velli, M., Dudok de Wit, T., Zank, G.P.: 2021, Parker Solar Probe enters the magnetically dominated solar corona. *Phys. Rev. Lett.* **127**, 255101. DOI. ADS.
- Katsikas, V., Exarhos, G., Moussas, X.: 2010, Study of the solar slow sonic, Alfvén, and fast magnetosonic transition surfaces. *Adv. Space Res.* **46**, 382. DOI. ADS.
- Keppens, R., Goedbloed, J.P.: 2000, Stellar winds, dead zones, and coronal mass ejections. *Astrophys. J.* **530**, 1036. DOI. ADS.
- Keto, E.: 2020, Stability and solution of the time-dependent Bondi-Parker flow. *Mon. Not. Roy. Astron. Soc.* **493**, 2834. DOI. ADS.
- King, J.H., Papitashvili, N.E.: 2005, Solar wind spatial scales in and comparisons of hourly Wind and ACE plasma and magnetic field data. *J. Geophys. Res.* **110**, A02104. DOI. ADS.

- Klein, K.G., Perez, J.C., Verscharen, D., Mallet, A., Chandran, B.D.G.: 2015, A modified version of Taylor's hypothesis for Solar Probe Plus observations. *Astrophys. J. Lett.* **801**, L18. DOI ADS.
- Kopp, R.A., Holzer, T.E.: 1976, Dynamics of coronal hole regions, I: Steady polytropic flows with multiple critical points. *Solar Phys.* **49**, 43. DOI ADS.
- Kraichnan, R.H.: 1965, Inertial-range spectrum of hydromagnetic turbulence. *Phys. Fluids* **8**, 1385. DOI ADS.
- Li, B., Li, X.: 2006, Effects of  $\alpha$  particles on the angular momentum loss from the Sun. *Astron. Astrophys.* **456**, 359. DOI ADS.
- Li, J.: 1999, Magnetic braking of the present Sun. *Mon. Not. Roy. Astron. Soc.* **302**, 203. DOI ADS.
- Li, J., Raymond, J.C., Acton, L.W., Kohl, J.L., Romoli, M., Noci, G., Naletto, G.: 1998, Physical structure of a coronal streamer in the closed-field region as observed from UVCS/SOHO and SXT/Yohkoh. *Astrophys. J.* **506**, 431. DOI ADS.
- Liewer, P.C., Neugebauer, M., Zurbuchen, T.: 2004, Characteristics of active-region sources of solar wind near solar maximum. *Solar Phys.* **223**, 209. DOI ADS.
- Lifschitz, A., Goedbloed, J.P.: 1997, Transonic magnetohydrodynamic flows. *J. Plasma Phys.* **58**, 61. DOI ADS.
- Linker, J.A., Mikić, Z., Biesecker, D.A., Forsyth, R.J., Gibson, S.E., Lazarus, A.J., Lecinski, A., Riley, P., Szabo, A., Thompson, B.J.: 1999, Magnetohydrodynamic modeling of the solar corona during Whole Sun Month. *J. Geophys. Res.* **104**, 9809. DOI ADS.
- Liu, Y.D., Chen, C., Stevens, M.L., Liu, M.: 2021, Determination of solar wind angular momentum and Alfvén radius from Parker Solar Probe observations. *Astrophys. J. Lett.* **908**, L41. DOI ADS.
- Liu, Y.D., Ran, H., Hu, H., Bale, S.D.: 2023, On the generation and evolution of switchbacks and the morphology of the Alfvénic transition: Low Mach-number boundary layers. *Astrophys. J.* **944**, 116. DOI ADS.
- Lloveras, D.G., Vázquez, A.M., Nuevo, F.A., Frazin, R.A.: 2017, Comparative study of the three-dimensional thermodynamical structure of the inner corona of solar minimum Carrington rotations 1915 and 2081. *Solar Phys.* **292**, 153. DOI ADS.
- Luhmann, J.G., Li, Y., Arge, C.N., Gazis, P.R., Ulrich, R.: 2002, Solar cycle changes in coronal holes and space weather cycles. *J. Geophys. Res.* **107**, 1154. DOI ADS.
- Lynch, B.J.: 2020, A model for coronal inflows and in/out pairs. *Astrophys. J.* **905**, 139. DOI ADS.
- MacGregor, K.B., Charbonneau, P.: 1994, Stellar winds with non-WKB Alfvén waves, I: Wind models for solar coronal conditions. *Astrophys. J.* **430**, 387. DOI ADS.
- Mackay, D.H., Yeates, A.R.: 2012, The Sun's global photospheric and coronal magnetic fields: Observations and models. *Liv. Rev. Solar Phys.* **9**, 6. DOI ADS.
- Marsch, E., Richter, A.K.: 1984, Distribution of solar wind angular momentum between particles and magnetic field: Inferences about the Alfvén critical point from Helios observations. *J. Geophys. Res.* **89**, 5386. DOI ADS.
- Martínez Pillet, V., Cauzzi, G., Tritschler, A., Harra, L., Andretta, A., Vourlidas, A., Raouafi, N., Alterman, B.L., Bellot Rubio, L., Cranmer, S.R., Gibson, S., De Groof, A., Habbal, S., Ko, Y.-K., Lepri, S.T., Linker, J., Malaspina, D.M., Matthews, S., Müller, D., Parenti, S., Petrie, G., Spadaro, D., Ugarte-Urra, I., Warren, H., Winslow, R., Zouganelis, I.: 2023, Solar physics in the 2020s: DKIST, Parker Solar Probe, and Solar Orbiter as a multi-messenger constellation. In: *The Era of Multi-Messenger Solar Physics*, IAU Symp. 372, in press.
- Mason, E.I., Antiochos, S.K., Viall, N.M.: 2019, Observations of solar coronal rain in null point topologies. *Astrophys. J. Lett.* **874**, L33. DOI ADS.
- Matsakos, T., Uribe, A., Königl, A.: 2015, Classification of magnetized star-planet interactions: Bow shocks, tail, and inspiraling flows. *Astron. Astrophys.* **578**, A6. DOI ADS.
- Matt, S., Pudritz, R.E.: 2005, Accretion-powered stellar winds as a solution to the stellar angular momentum problem. *Astrophys. J. Lett.* **632**, L135. DOI ADS.
- Matt, S., Pudritz, R.E.: 2008, Accretion-powered stellar winds, II: Numerical solutions for stellar wind torques. *Astrophys. J.* **678**, 1109. DOI ADS.
- Matthaeus, W.H.: 1997, Turbulence properties along the Solar Probe trajectory. In: S. Habbal (ed.), *Robotic Exploration Close to the Sun: Scientific Basis*, CP-385, AIP, Melville, 67. DOI ADS.
- Moraes Filho, V., Uritsky, V., Thompson, B. J., DeForest, C.: 2022, SynCOM: A dynamic model for flow tracking algorithms. *AGU Fall Meeting*, abs. SH12C-1466. ADS.
- Neugebauer, M., Snyder, C.W.: 1962, Solar plasma experiment. *Science* **138**, 1095. DOI ADS.

- Newmark, J.S., Gopalswamy, N., Kim, Y.H., Viall, N.M., Cho, K.S.F., Reginald, N.L., Bong, S.C., Gong, Q., Choi, S., Strachan, L., Yashiro, S.: 2020, The Coronal Diagnostic Experiment (CODEX). *AGU Fall Meeting*, abstract SH028-0011. [ADS](#).
- Owocki, S.P.: 2009, Stellar magnetospheres. In: C. Neiner, J.-P. Zahn (eds.), *Stellar Magnetism*, *EAS Pub. Ser.*, **39**, EDP, Les Ulis, 223. [DOI](#). [ADS](#).
- Parker, E.N.: 1958, Dynamics of the interplanetary gas and magnetic fields. *Astrophys. J.* **128**, 664. [DOI](#). [ADS](#).
- Parker, E.N.: 1964, Dynamical properties of stellar coronas and stellar winds, I: Integration of the momentum equation. *Astrophys. J.* **139**, 72. [DOI](#). [ADS](#).
- Pecora, F., Yang, Y., Gibson, S.E., Viall, N.M., Chhiber, R., DeForest, C.E., Matthaeus, W.H.: 2023, Magnetohydrodynamic turbulence simulations: A testing ground for PUNCH. *Solar Phys.*, in preparation.
- Pineda, J.S., Villadsen, J.: 2023, Coherent radio bursts from known M-dwarf planet-host YZ Ceti. *Nature Astron.* **7**, 569. [DOI](#). [ADS](#).
- Pinto, R.F., Brun, A.S., Jouve, L., Grappin, R.: 2011, Coupling the solar dynamo and the corona: Wind properties, mass, and momentum losses during an activity cycle. *Astrophys. J.* **737**, 72. [DOI](#). [ADS](#).
- Pizzo, V., Schwenn, R., Marsch, E., Rosenbauer, H., Mühlhäuser, K.-H., Neubauer, F.M.: 1983, Determination of the solar wind angular momentum flux from the Helios data: An observational test of the Weber and Davis theory. *Astrophys. J.* **271**, 335. [DOI](#). [ADS](#).
- Pneuman, G.W., Kopp, R.A.: 1971, Gas-magnetic field interactions in the solar corona. *Solar Phys.* **18**, 258. [DOI](#). [ADS](#).
- Pulupa, M., Bale, S.D., Bonnell, J.W., Bowen, T.A., Carruth, N., Goetz, K., Gordon, D., Harvey, P.R., Maksimovic, M., Martínez-Oliveros, J.C., Moncuquet, M., Saint-Hilaire, P., Seitz, D., Sundkvist, D.: 2017, The Solar Probe Plus Radio Frequency Spectrometer: Measurement requirements, analog design, and digital signal processing. *J. Geophys. Res.* **122**, 2836. [DOI](#). [ADS](#).
- Raouafi, N.E., Matteini, L., Squire, J., Badman, S.T., Velli, M., Klein, K.G., Chen, C.H.K., Matthaeus, W.H., Szabo, A., Linton, M., Allen, R.C., Szalay, J.R., Bruno, R., Decker, R.B., Akhavan-Tafti, M., Agapitov, O.V., Bale, S.D., Banyopadhyay, R., Battams, K., Bercić, L., Bourouaine, S., Bowen, T.A., Cattell, C., Chandran, B.D.G., Chhiber, R., Cohen, C.M.S., D'Amicis, R., Giacalone, J., Hess, P., Howard, R.A., Horbury, T.S., Jagarlamudi, V.K., Joyce, C.J., Kasper, J.C., Kinnison, J., Laker, R., Liewer, P., Malaspina, D.M., Mann, I., McComas, D.J., Niembro-Hernandez, T., Nieves-Chinchilla, T., Panasenco, O., Pokorný, P., Pusack, A., Pulupa, M., Perez, J.C., Riley, P., Rouillard, A.P., Shi, C., Stenborg, G., Tenerani, A., Verniero, J.L., Viall, N., Vourlidas, A., Wood, B.E., Woodham, L.D., Woolley, T.: 2023, Parker Solar Probe: Four years of discoveries at solar cycle minimum. *Space Sci. Rev.* **219**, 8. [DOI](#). [ADS](#).
- Reiss, M.A., MacNeice, P.J., Mays, L.M., Arge, C.N., Möstl, C., Nikolic, L., Amerstorfer, T.: 2019, Forecasting the ambient solar wind with numerical models, I: On the implementation of an operational framework. *Astrophys. J. Suppl.* **240**, 35. [DOI](#). [ADS](#).
- Réville, V., Brun, A.S.: 2017, Global solar magnetic field organization in the outer corona: Influence on the solar wind speed and mass flux over the cycle. *Astrophys. J.* **850**, 45. [DOI](#). [ADS](#).
- Riley, P., Linker, J.A., Mikić, Z., Lionello, R., Ledvina, S.A., Luhmann, J.G.: 2006, A comparison between global solar magnetohydrodynamic and potential field source surface model results. *Astrophys. J.* **653**, 1510. [DOI](#). [ADS](#).
- Riley, P., Lionello, R.: 2011, Mapping solar wind streams from the Sun to 1 AU: A comparison of techniques. *Solar Phys.* **270**, 575. [DOI](#). [ADS](#).
- Ruffolo, D., Matthaeus, W.H., Chhiber, R., Usmanov, A.V., Yang, Y., Bandyopadhyay, R., Parashar, T.N., Goldstein, M.L., DeForest, C.E., Wan, M., Chasapis, A., Maruca, B.A., Velli, M., Kasper, J.C.: 2020, Shear-driven transition to isotropically turbulent solar wind outside the Alfvén critical zone. *Astrophys. J.* **902**, 94. [DOI](#). [ADS](#).
- Sakurai, T.: 1985, Magnetic stellar winds: A 2-D generalization of the Weber-Davis model. *Astron. Astrophys.* **152**, 121. [ADS](#).
- Sakurai, T.: 1990, Magnetohydrodynamic solar/stellar wind models. *Comput. Phys. Rep.* **12**, 247. [DOI](#). [ADS](#).
- Sanchez-Diaz, E., Rouillard, A.P., Davies, J.A., Lavraud, B., Sheeley, N.R., Pinto, R.F., Kilpua, E., Plotnikov, I., Genot, V.: 2017, Observational evidence for the associated formation of blobs and raining inflows in the solar corona. *Astrophys. J. Lett.* **835**, L7. [DOI](#). [ADS](#).

- Saur, J., Grambusch, T., Duling, S., Neubauer, F.M., Simon, S.: 2013, Magnetic energy fluxes in sub-Alfvénic planet star and moon planet interactions. *Astron. Astrophys.* **552**, A119. DOI. ADS.
- Savage, S.L., McKenzie, D.E., Reeves, K.K.: 2012, Re-interpretation of supra-arcade downflows in solar flares. *Astrophys. J. Lett.* **747**, L40. DOI. ADS.
- Schatten, K.H., Wilcox, J.M., Ness, N.F.: 1969, A model of interplanetary and coronal magnetic fields. *Solar Phys.* **6**, 442. DOI. ADS.
- Scherrer, P.H., Bogart, R.S., Bush, R.I., Hoeksema, J.T., Kosovichev, A.G., Schou, J., Rosenberg, W., Springer, L., Tarbell, T.D., Title, A., Wolfson, C.J., Zayer, I., MDI Engineering Team: 1995, The Solar Oscillations Investigation: Michelson Doppler Imager. *Solar Phys.* **162**, 129. DOI. ADS.
- Schwadron, N.A., Connick, D.E., Smith, C.: 2010, Magnetic flux balance in the heliosphere. *Astrophys. J. Lett.* **722**, L132. DOI. ADS.
- Sheeley, N.R., Wang, Y.-M.: 2014, Coronal inflows during the interval 1996–2014. *Astrophys. J.* **797**, 10. DOI. ADS.
- Sheeley, N.R., Wang, Y.-M., Hawley, S.H., Brueckner, G.E., Dere, K.P., Howard, R.A., Koomen, M.J., Korendyke, C.M., Michels, D.J., Paswaters, S.E., Socker, D.G., St. Cyr, O.C., Wang, D., Lamy, P.L., Llebaria, A., Schwenn, R., Simnett, G.M., Plunkett, S., Biesecker, D.A.: 1997, Measurements of flow speeds in the corona between 2 and 30  $R_{\odot}$ . *Astrophys. J.* **484**, 472. DOI. ADS.
- Shkolnik, E., Bohlender, D.A., Walker, G.A.H., Collier Cameron, A.: 2008, The on-off nature of star-planet interactions. *Astrophys. J.* **676**, 628. DOI. ADS.
- Shodhan, S., Crooker, N.U., Kahler, S.W., Fitzenreiter, R.J., Larson, D.E., Lepping, R.P., Siscoe, G.L., Gosling, J.T.: 2000, Counterstreaming electrons in magnetic clouds. *J. Geophys. Res.* **105**, 27261. DOI. ADS.
- Skumanich, A.: 1972, Time scales for Ca II emission decay, rotational braking, and lithium depletion. *Astrophys. J.* **171**, 565. DOI. ADS.
- Smith, C.W., Schwadron, N.A., DeForest, C.E.: 2013, Decline and recovery of the interplanetary magnetic field during the protracted solar minimum. *Astrophys. J.* **775**, 59. DOI. ADS.
- Sturrock, P.A., Hartle, R.E.: 1966, Two-fluid model of the solar wind. *Phys. Rev. Lett.* **16**, 628. DOI. ADS.
- Suess, S.T.: 1982, Unsteady, thermally conductive coronal flow. *Astrophys. J.* **259**, 880. DOI. ADS.
- Suess, S.T., Wang, A.-H., Wu, S.T., Poletto, G., McComas, D.J.: 1999, A two-fluid, MHD coronal model. *J. Geophys. Res.* **104**, 4697. DOI. ADS.
- Tasnim, S., Cairns, I.H.: 2016, An equatorial solar wind model with angular momentum conservation and nonradial magnetic fields and flow velocities at an inner boundary. *J. Geophys. Res.* **121**, 4966. DOI. ADS.
- Tasnim, S., Cairns, I.H., Li, B., Wheatland, M.S.: 2019, Mapping magnetic field lines for an accelerating solar wind. *Solar Phys.* **294**, 155. DOI. ADS.
- Tasnim, S., Cairns, I.H., Wheatland, M.S.: 2018, A generalized equatorial model for the accelerating solar wind. *J. Geophys. Res.* **123**, 1061. DOI. ADS.
- Taylor, G.I.: 1938, The spectrum of turbulence. *Proc. Roy. Soc. London A* **164**, 476. DOI. ADS.
- Telloni, D., Andretta, V., Antonucci, E., Bemporad, A., Capuano, G.E., Fineschi, S., Giordano, S., Habbal, S., Perrone, D., Pinto, R.F., Sorriso-Valvo, L., Spadaro, D., Susino, R., Woodham, L.D., Zank, G.P., Romoli, M., Bale, S.D., Kasper, J.C., Auchère, F., Bruno, R., Capobianco, G., Case, A.W., Casini, C., Casti, M., Chioetto, P., Corso, A.J., Da Deppo, V., De Leo, Y., Dudok de Wit, T., Frassati, F., Frassetto, F., Goetz, K., Guglielmino, S.L., Harvey, P.R., Heinzl, P., Jerse, G., Korreck, K.E., Landini, F., Larson, D., Liberatore, A., Livi, R., MacDowall, R.J., Magli, E., Malaspina, D.M., Massone, G., Messerotti, M., Moses, J.D., Naletto, G., Nicolini, G., Nisticò, G., Panasenco, O., Pancrazzi, M., Pelizzo, M.G., Pulupa, M., Reale, F., Romano, P., Sasso, C., Schühle, U., Stangalini, M., Stevens, M.L., Strachan, L., Straus, T., Teriaca, L., Uslenghi, M., Velli, M., Verscharen, D., Volpicelli, C.A., Whittlesey, P., Zangrilli, L., Zimbardo, G., Zuppella, P.: 2021, Exploring the solar wind from its source on the corona into the inner heliosphere during the first Solar Orbiter–Parker Solar Probe quadrature. *Astrophys. J. Lett.* **920**, L14. DOI. ADS.
- Tenerani, A., Velli, M., DeForest, C.E.: 2016, Inward motions in the outer solar corona between 7 and 12  $R_{\odot}$ : Evidence for waves or magnetic reconnection jets? *Astrophys. J. Lett.* **825**, L3. DOI. ADS.

- Townsend, R.H.D., Oksala, M.E., Cohen, D.H., Owocki, S.P., ud-Doula, A.: 2010, Discovery of rotational braking in the magnetic helium-strong star sigma Orionis E. *Astrophys. J. Lett.* **714**, L318. DOI ADS.
- ud-Doula, A.: 2017, Magnetic fields in massive stars and magnetically confined winds. *Astron. Nachrichten* **338**, 944. DOI ADS.
- Usmanov, A.V., Matthaeus, W.H., Goldstein, M.L., Chhiber, R.: 2018, The steady global corona and solar wind: A three-dimensional MHD simulation with turbulence transport and heating. *Astrophys. J.* **865**, 25. DOI ADS.
- Vázquez, A.M., van Ballegooijen, A.A., Raymond, J.C.: 2003, The effect of proton temperature anisotropy on the solar minimum corona and wind. *Astrophys. J.* **598**, 1361. DOI ADS.
- Velli, M.: 1993, On the propagation of ideal, linear Alfvén waves in radially stratified stellar atmospheres and winds. *Astron. Astrophys.* **270**, 304. ADS.
- Velli, M.: 1994, From supersonic winds to accretion: Comments on the stability of stellar winds and related flows. *Astrophys. J. Lett.* **432**, L55. DOI ADS.
- Velli, M.: 2001, Hydrodynamics of the solar wind expansion. *Astrophys. Space Sci.* **277**, 157. DOI ADS.
- Verscharen, D., Bale, S.D., Velli, M.: 2021a, Flux conservation, radial scalings, Mach numbers, and critical distances in the solar wind: Magnetohydrodynamics and Ulysses observations. *Mon. Not. Roy. Astron. Soc.* **506**, 4993. DOI ADS.
- Verscharen, D., Stansby, D., Finley, A.J., Owen, C.J., Horbury, T., Maksimovic, M., Velli, M., Bale, S.D., Louarn, P., Fedorov, A., Bruno, R., Livi, S., Khotyaintsev, Y.V., Vecchio, A., Lewis, G.R., Anekallu, C., Kelly, C.W., Watson, G., Kataria, D.O., O'Brien, H., Evans, V., Angelini, V., Solar Orbiter SWA, MAG, and RPW Teams: 2021b, The angular-momentum flux in the solar wind observed during Solar Orbiter's first orbit. *Astron. Astrophys.* **656**, A28. DOI ADS.
- Viall, N.M., DeForest, C.E., Kepko, L.: 2021, Mesoscale structure in the solar wind. *Front. Astron. Space Sci.* **8**, 139. DOI ADS.
- Vidotto, A.A.: 2021, The evolution of the solar wind. *Liv. Rev. Solar Phys.* **18**, 3. DOI ADS.
- Weber, E.J., Davis, L., Jr.: 1967, The angular momentum of the solar wind. *Astrophys. J.* **148**, 217. DOI ADS.
- Wexler, D.B., Stevens, M.L., Case, A.W., Song, P.: 2021, Alfvén speed transition zone in the solar corona. *Astrophys. J. Lett.* **919**, L33. DOI ADS.
- Xu, F., Borovsky, J.E.: 2015, A new four-plasma categorization scheme for the solar wind. *J. Geophys. Res.* **120**, 70. DOI ADS.
- Zank, G.P., Zhao, L.-L., Adhikari, L., Telloni, D., Kasper, J.C., Stevens, M., Rahmati, A., Bale, S.D.: 2022, Turbulence in the sub-Alfvénic solar wind. *Astrophys. J. Lett.* **926**, L16. DOI ADS.
- Zhang, J., Huang, S.Y., Yuan, Z.G., Jiang, K., Xu, S.B., Bandyopadhyay, R., Wei, Y.Y., Xiong, Q.Y., Wang, Z., Yu, L., Lin, R.T.: 2022, Higher-order turbulence statistics in sub-Alfvénic solar wind observed by Parker Solar Probe. *Astrophys. J.* **937**, 70. DOI ADS.
- Zhao, L.-L., Zank, G.P., Telloni, D., Stevens, M., Kasper, J.C., Bale, S.D.: 2022, The turbulent properties of the sub-Alfvénic solar wind measured by the Parker Solar Probe. *Astrophys. J. Lett.* **928**, L15. DOI ADS.
- Zhao, X.P., Hoeksema, J.T.: 2010, The magnetic field at the inner boundary of the heliosphere around solar minimum. *Solar Phys.* **266**, 379. DOI ADS.